Novel Zeolitic Imidazolate Framework/Polymer Membranes for Hydrogen Separations in Coal Processing

Final Report

Reporting Period Start Date: February 1, 2009
Reporting Period End Date: January 31, 2013

Inga H. Musselman (Principal Investigator)

May 1, 2013

DE-NT0007636

Department of Chemistry
The University of Texas at Dallas
800 W. Campbell Rd.
Richardson, TX 75080

DISCLAIMER

ABSTRACT

Nanoparticles of zeolitic imidazolate frameworks and other related hybrid materials were prepared by modifying published synthesis procedures by introducing bases, changing stoichiometric ratios, or adjusting reaction conditions. These materials were stable at temperatures >300 °C and were compatible with the polymer matrices used to prepare mixed-matrix membranes (MMMs). MMMs tested at 300 °C exhibited a >30 fold increase in permeability, compared to those measured at 35 °C, while maintaining H_2/CO_2 selectivity. Measurements at high pressure (up to 30 atm) and high temperature (up to 300 °C) resulted in an increase in gas flux across the membrane with retention of selectivity. No variations in permeability were observed at high pressures at either 35 or 300 °C. CO_2-induced plasticization was not observed for Matrimid®, VTEC, and PBI polymers or their MMMs at 30 atm and 300 °C. Membrane surface modification by cross-linking with ethylenediamine resulted in an increase in H_2/CO_2 selectivity at 35 °C. Spectrometric analysis showed that the cross-linking was effective to temperatures <150 °C. At higher temperatures, the cross-linked membranes exhibit a H_2/CO_2 selectivity similar to the uncross-linked polymer.

TABLE OF CONTENTS

INTRODUCTION

The replacement of energy intensive separations with membranes should result in an energy savings as well as an economic savings. The ability to fabricate membranes with selective additives should retain the advantages of the polymer matrix including flexibility and module design.

The overall objectives of the proposed research were to prepare novel mixed-matrix membranes based on composites of polymers and nanoparticles of zeolitic imidazolate frameworks (ZIF) and related hybrid frameworks. Membranes containing these new materials were used to evaluate separations important to coal gasification (e.g. H_2, CO, O_2, CO_2). The goal was to exploit the high surface areas, adsorption capacities, and selectivities of the nanoporous ZIF additives to achieve unprecedented transport of gases [1].

The organization of this final report follows the proposed project management plan, where the major tasks are listed. The *experimental* section describes the synthesis of the proposed ZIFs and related hybrid materials, the synthesis of non-commercially available polymers, and membrane preparation. Due to the extensive number of ZIF/polymer systems, the *results and discussion* section is organized by the polymer matrix. This section also includes the results of membranes tested at high temperatures and high pressures. Finally, a section listing the scientific and educational *outcomes/impacts* of the project is included.

EXECUTIVE SUMMARY

Our strategy to improve the permeability and selectivity of polymer membranes was to incorporate ZIFs and related hybrid frameworks into polymer matrices. These porous materials are chemically and thermally stable at DOE 2015 target conditions. Additionally, they possess pore apertures small enough to perform molecular sieving of gas mixtures (i.e. H_2/CO_2, H_2/CO, CO/CO_2, and H_2/CH_4). In addition to these properties, ZIFs, which contain organic ligands, are more compatible with polymer matrices than are zeolites. Among the large variety of ZIFs, metal-organic frameworks (MOFs), and other hybrid materials that have been reported in the open literature, we identified ZIF-7, ZIF-8, ZIF-20, ZIF-90, ZIF-95, MIL-53, NH_2-MIL-53, and MOP-18 as materials suitable for gas separations. We purchased (ZIF-8 and MIL-53) or synthesized nanocrystals of these ZIFs and MOFs in our lab.

We chose polymers with T_gs above 300 °C to prepare mixed-matrix membranes (MMMs) for operation at DOE 2015 target conditions. Polymers such as Matrimid®, PBI, and VTEC are commercially available, but other polymers such as PIM-1 and the 6FDA derivatives were synthesized in our lab.

Other strategies to improve gas separation were also investigated. The cross-linking of polymer membranes with ethylenediamine (EDA) was applied to 6FDA and Matrimid® polymer membranes and their MMMs. The EDA cross-linking proved to be effective to improve the H_2/CO_2 selectivity of the membranes. Separation factors of 144 were obtained for H_2/CO_2 with EDA cross-linked 6FDA-durene membranes with a H_2 permeability of 52 Barrers at 35 °C and 3 atm. The stability of this chemical modification was examined to determine its applicability in high temperature, high pressure gas separations. The results showed that EDA cross-linking reverses at temperatures above 150 °C with a loss of selectivity. Therefore, these membranes were not tested at high temperature. Another strategy to improve the gas transport properties of the prepared membranes was to coat the MMM surface with a thin (<3 μm), highly selective polymer layer that controls gas flux across the membrane. Since very thin and mechanically stable polymer membranes are difficult to prepare, this strategy solves this problem by combining the MMM and the highly selective polymer layer.

We tested flat membranes at DOE 2015 target conditions of up to 300 °C and 30 atm in a high pressure, high temperature permeameter (HPHT) that we built as part of this project. Permeabilities of H_2, CO_2, and N_2 were obtained for selected membranes. Permeability results at 300 °C and 30 atm demonstrate that the polymers and MMMs are mechanically and thermally stable even after prolonged exposure (>300 h) to gases. VTEC, Matrimid®, and PBI membranes retained their selectivity properties when the temperature was increased from 35 to 300 °C. Permeability, however, increased with increasing temperature and 35-fold increments in H_2 permeability were observed for VTEC membranes when the temperature was increased from 35 to 300 °C. Pressure increments from 3 to 30 atm at 35 °C and at 300 °C resulted in an increased flux across the membrane without changes in permeability. These results indicate that the membranes were free from defects as well as mechanically stable at these extreme conditions. ZIF-8/PBI MMMs also showed significant changes in permeability with increasing temperature. The MMMs showed an increase in H_2 permeability from 5.4 Barrers (35 °C) to 397 Barrers (300 °C), while retaining a H_2/CO_2 selectivity of 14. It was also discovered that CO_2-induced plasticization of the membrane could be mitigated by increasing the temperature. As was observed for Matrimid® and MOP-18/Matrimid® MMMs, when the temperature was increased from 35 to 70 °C, the H_2/CO_2 selectivity was recovered. The reduction of the plasticization is attributed to the increase of the required plasticization pressure when the temperature is increased to 70 °C. In the case of Matrimid®, the plasticization pressure was increased from 30 atm at 35 °C to >30 atm at 70 °C. It is also worth noting that plasticization was not observed for VTEC and PBI membranes in the range of pressures and temperatures at which these materials were tested.

EXPERIMENTAL METHODS

ZIF and related hybrid framework materials

ZIF synthesis

Thermally and chemically stable ZIFs with high affinity and selectivity for H_2 and CO_2 were synthesized and used to prepare MMMs. Commercially available ZIF-8 (Basolite® Z1200, Sigma Aldrich) was activated by heating in a vacuum oven at 100 °C for 1 d. ZIF-7 [2, 3], ZIF-8 [4], ZIF-20 [3], ZIF-90 [5], and ZIF-95 [6] crystals were synthesized by modifying published procedures.

MOF and MOP-18 synthesis

Commercially available MIL-53 (Basolite® A100, Sigma Aldrich) was used as received. MIL-53 [7, 8], NH_2-MIL-53 [8], and MOP-18 [9] crystals were synthesized according to published procedures.

Polymers

Matrimid®-5218 soluble polyimide (Huntsman Corporation), 26% (w/w) polybenzimidazole in dimethylacetamide with 1.5% (w/w) LiCl (PBI Performance Products, Inc), and VTEC PI-1388 (RBI, Inc) were used as received.

PIM-1

Following reported procedures [10, 11], the Polymer of Intrinsic Microposrosity-1 (PIM-1) was synthesized from dried and purified monomers (Figure 1).

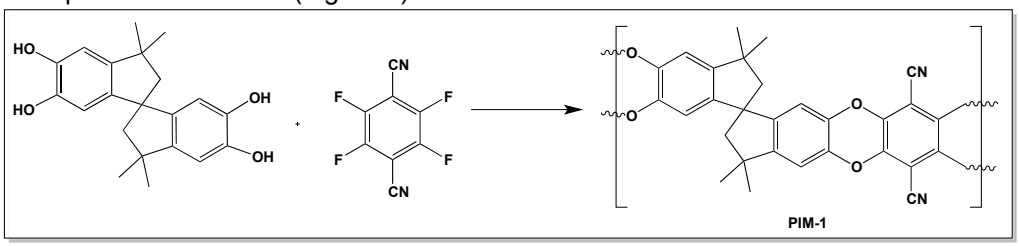

Figure 1. Synthetic scheme for the PIM-1 polymer.

6FDA-ODA/NDA polymers

Following reported procedures, [10, 12, 13] five polyimides from 4,4'-hexafluoroisopropylidene bisphthalic dianhydride (6FDA) and 2 diamines (4,4'-oxydianiline, ODA, and 1,5-diaminonaphthalene, NDA) were synthesized. The anhydride was dried under vacuum, while the diamines were purified by sublimation at 150 mtorr prior to use. 6FDA-NDA, 6FDA-ODA, and their copolymers (3:1, 1:1, 1:3 molar ratios) were prepared via the initial formation of a polyamic acid followed by chemical imidization using triethylamine/acetic anhydride (Figure 2).

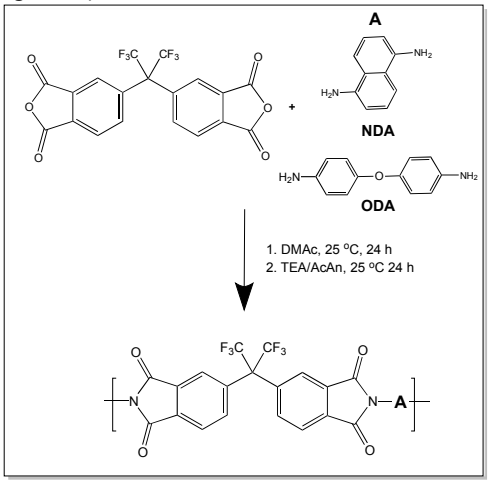

Figure 2. Scheme for the synthesis of 6FDA-based polyimides.

6FDA-durene

Synthesis of 6FDA-durene was carried out using a modified literature procedure [14]. Care was taken to minimize the amount of water in the reaction mixture by drying all glassware prior to use and conducting the reaction under a flow of nitrogen. 6FDA (0.003 mol, 1.33g) was added to durene-diamine (0.003mol, 0.49g) in DMAc (7.8 mL) in a three-necked round-bottom flask fitted to a condenser to obtain a 20 wt% monomer concentration. The mixture was stirred at 50 ^{o}C for 2 h under a nitrogen purge to obtain polyamic acid. Next, a 1:1 molar mixture of triethylamine (0.012mol, 1.7mL) and acetic anhydride (0.012mol, 1.2mL) was added (four times the number of moles of 6FDA). The mixture was stirred at 50 ^{o}C for 1 h, 75 ^{o}C for 1 h and 100 ^{o}C for 30 min under a nitrogen purge. The polymer was precipitated in methanol, washed several times with methanol, and dried at 150 ^{o}C under vacuum for 1 d.

6FDA-DAM-DABA polymers

PDMC (Propanediol esterified 6FDA-DAM-DABA, Figure 3) was synthesized using published literature procedures [15, 16].

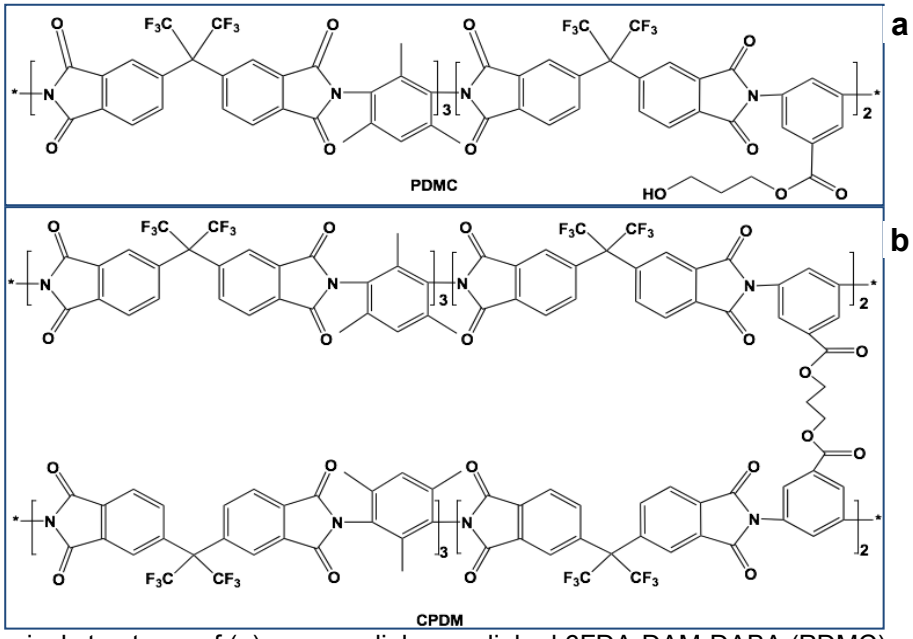

Figure 3. Chemical structures of (a) propanediol cross-linked 6FDA-DAM-DABA (PDMC) and (b) cross-linked propanediol esterified 6FDA-DAM-DABA (CPDM).

Membrane preparation

Matrimid®-based MMMs

MMMs containing 25-300% (w/w) ZIF (or related hybrid frameworks, i.e., MIL-53 and MOP-18) in Matrimid® were fabricated by preparing a dispersion of ZIF or other hybrid framework in $CHCl_3$ or THF and a solution of the polymer in the same solvent. The additive dispersion was alternately bath sonicated and stirred (6 cycles, 15 min each time) to obtain a homogenous dispersion. Sonication breaks up particle aggregates and enhances homogeneity. Afterwards, 20% of the polymer solution was added to the additive dispersion as a pre-coating step. To further enhance mixing, the dispersion was subjected to a LabRAM Mixer (Resodyn™ Acoustic Mixers, Inc., purchased with matching funds for this project) set at 20% intensity for 20 min. The additive/Matrimid® dispersion was concentrated by evaporating the solvent until the polymer concentration was 10% by weight. The dispersion was cast onto a glass substrate using an automatic film applicator (Sheen Instruments, Ltd., 1133N) equipped with an adjustable blade (Sheen Instruments, Ltd., 1117). The resulting membranes were peeled off the substrate and annealed at 100 ^{o}C (MOP-18 and MIL-53/Matrimid® MMMs), 100 °C (ZIF-7/Matrimid® MMMs), or 240 °C (ZIF-8/Matrimid® MMMs) for 1 d prior to further characterization and testing.

PIM-1-based MMMs
Metal-organic framework nanocrystals (MIL-53, ZIF-8, and ZIF-90) were incorporated into PIM-1 at loadings up to 17.6% (w/w). The preparation of these membranes followed the same steps described in the preparation of Matrimid®-based MMMs using $CHCl_3$ as the solvent. The resulting membranes were annealed at 60 °C for 1 d.

6FDA-ODA/NDA-based MMMs
Several MMMs comprising the synthesized thermally stable polymers and ZIFs or MOFs were prepared. A 25% (w/w) ZIF-8/6FDA-NDA MMM was fabricated using ZIF-8 particles having different particle sizes, including commercially available ZIF-8 (Basolite® Z1200, 120-nm particles) and synthesized ZIF-8 (60-nm and 111-nm particle sizes). The additives and polymers were dispersed in DMF, and stirring and sonication protocols for Matrimid®-based MMMs were followed. The solutions were cast on a glass substrate, dried, and annealed following a temperature program prior to further characterization and testing.

6FDA-DAM-DABA-based MMMs
ZIF-8 (50% (w/w)/PDMC MMMs were fabricated and cross-linked by annealing at 280 °C for 1d.

MMM-EDA surface modification
EDA (20 mL) was equilibrated in a tightly capped 1000 mL glass jar for 6 h. Annealed ZIF-8/6FDA-durene and MIL-53/Matrimid® MMMs were suspended in the EDA vapor for 40 min at 35 °C and then immediately washed with deionized water to remove any unreacted EDA. Finally, these MMMs were dried at 70 °C for 1 d under vacuum.

ZIF-8/PBI MMMs
Following Matrimid®-based membrane preparation protocols, PBI-based MMMs containing different weight loadings of Basolite® Z1200 (ZIF-8) were fabricated as flexible membranes. Due to the high boiling point solvent used (DMAc), the MMMs were promptly placed in a heated chamber at 50 °C under a N_2 purge for at least 5 h. Afterwards, the MMMs were removed from the glass substrate and dried under vacuum following a temperature program (80 °C, 150 °C, and 220 °C for 1 d each).

PBI spin-coated MMMs
A volume of 0.1 µL of 7 wt% PBI/DMAc solution was deposited onto ZIF-8/PBI MMMs during spinning at 500 or 1000 rpm for 60 s. After drying in air for 12 h, the membrane was heated in a vacuum oven at 50 °C for 5 h, then at 80 °C for 5 h, 120 °C for 5 h, 170 °C for 5 h, and finally at 220 °C for 1 d.

VTEC PI-1388 membranes
A 12 wt% VTEC PI-1388 polyamic acid solution was prepared by stirring for 15 h in *N*,*N*-dimethylacetamide. The solution was cast onto a Mylar® sheet at room temperature using an automatic film applicator (Sheen 1133N) with a calibrated doctor blade. The membrane, still on the Mylar® sheet, was transferred to a nitrogen purged chamber where it dried for 5 h at 80 °C. High temperatures and long periods of time are required to induce imidization of the polyamic acid. Therefore, the membrane was removed from the Mylar® sheet and heated in a vacuum oven first at 80 °C for 2 d, then at 150 °C for 1 d, and finally at 250 °C for 2 d, followed by cooling to room temperature.

Characterization of ZIFs and MMMs
The ZIFs, MOFs, MOP-18, polymer films, and MMMs were characterized using a variety of analytical techniques. To determine the crystallinity of the material, X-ray diffraction (XRD) patterns were acquired from 3 to 45° 2θ at a rate of 0.04°/s with a Rigaku Ultima IV diffractometer using Cu Kα X-ray radiation. A Nicolet 360 Fourier transform infrared (FTIR) spectrometer was used to record IR spectra at room temperature in the range of 400-4000 cm^{-1} of powders (as a KBr pellet), and polymer and MMM films (using an attenuated total reflectance (ATR) accessory equipped with a diamond crystal). Thermogravimetric analyses (TGA) of the powders and films were conducted under N_2 using a Perkin Elmer Pyris-1 instrument with a temperature program from 90 to 1000 °C at a heating rate of 10 °C/min.

A Zeiss Supra 40 field emission scanning electron microscope (FE-SEM) operated at 10 keV was used to acquire secondary electron images of the materials. Before imaging, samples were mounted on carbon tape adhered to aluminum stubs and coated with 10 nm of Au/Pd using a Technics Hummer VI Sputtering System. To prepare cross-sections of the polymer films and MMMs, the membranes were freeze-fractured after immersing them in liquid N_2 for 2 min. Differential scanning calorimetry (DSC) results for the polymer films and MMMs were obtained using a Mettler Toledo DSC1 Star^e System. The thermograms were recorded under N_2 from 200 to 450 °C at 10 °C/min. The T_g of the MMMs were obtained from the 4th run of the DSC analysis. The T_g is determined by fitting straight lines to the temperature versus heat flow curve before, during, and after taking the points of intersection at the onset and endpoint of transition. The T_g is taken as one-half the change in heat capacity between the onset and the endpoint.

High pressure, high temperature instrument

The HPHT permeameter was built according the diagram shown in Figure 4 using matching funds for this project [17]. Figure 4 shows the main components (pressure transducers, thermocouples, metering valves, and reservoirs). A LabView front panel that controls the instrument was also developed.

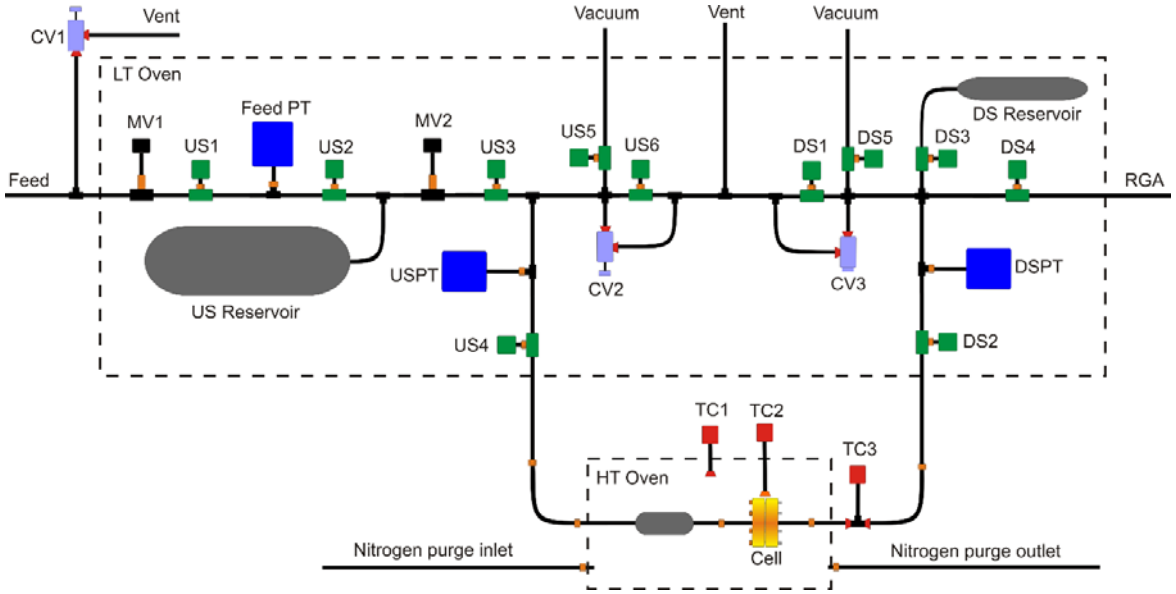

Figure 4. Schematic diagram of the HPHT permeameter. DS = high pressure downstream valve, US = high pressure upstream valve, MV = metering valve, CV = check valve, TC = thermocouple, PT = pressure transducer.

Membrane testing

Low pressure, low temperature (2.5 atm and 35 °C) gas permeation measurements of the prepared membranes were performed using custom made permeameters at constant volume. High pressure, high temperature gas permeation measurements (up to 30 atm and up to 300 °C) were performed with the HPHT permeameter.

RESULTS AND DISCUSSION

ZIFs and related hybrid frameworks

ZIF-7

Figure 5 shows a SEM image of ZIF-7 particles. The particles are 60 to 70 nm in diameter with no defined morphology. The XRD pattern of the synthesized particles shows the peaks expected for ZIF-7 (Figure 6).

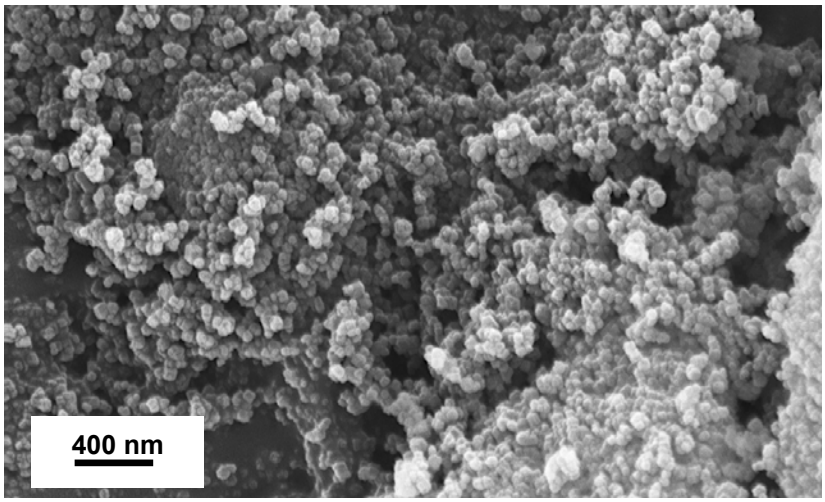

Figure 5. SEM image of ZIF-7 nanoparticles.

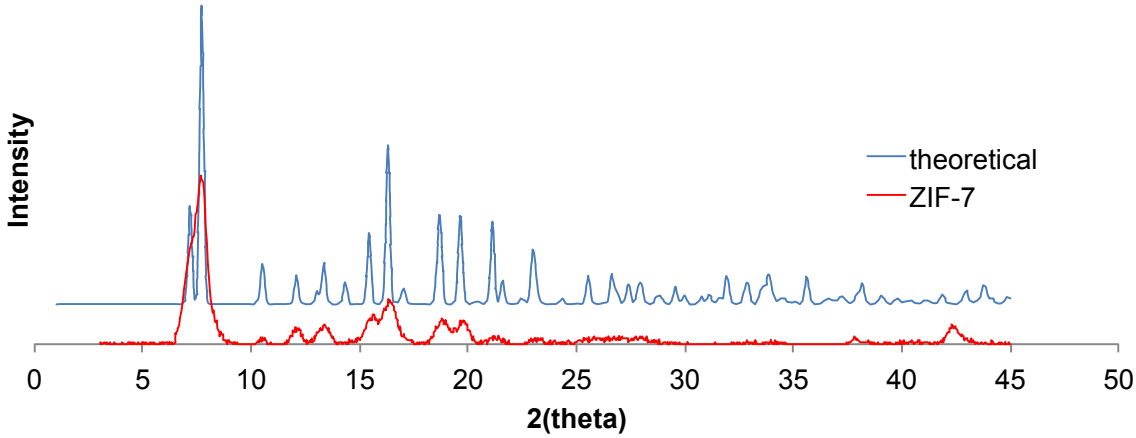

Figure 6. XRD pattern of synthesized ZIF-7 particles.

ZIF-8

Nano-sized ZIF-8 particles were obtained upon the addition of TEA to the synthesis mixture [18]. SEM images of this material show particles that are 60 ± 4 nm in diameter (Figure 7). XRD analysis of the synthesized particles showed the expected peaks for ZIF-8 (Figure 8).

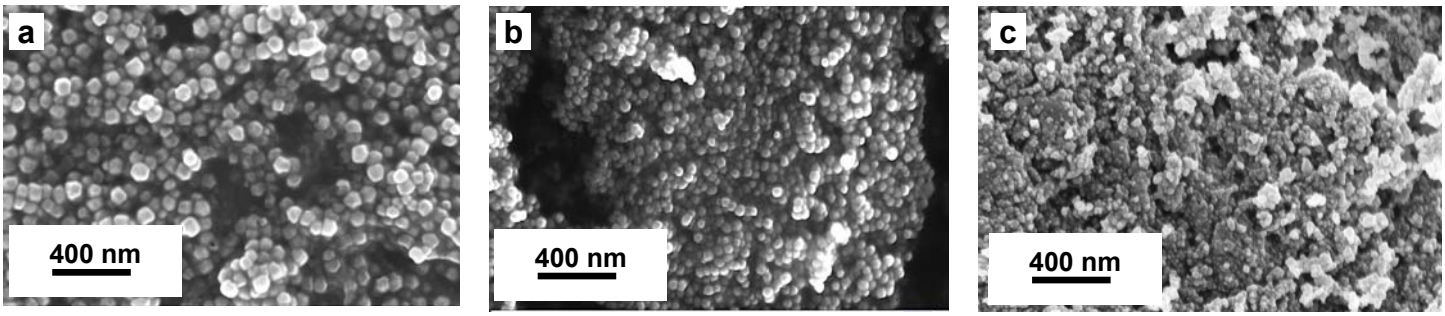

Figure 7. SEM analysis of ZIF-8 nanocrystals: (a) commercially available ZIF-8 (Basolite®, 120±18 nm), ZIF-8 (b) synthesized without TEA (Batch 1, 111±21 nm), and (c) synthesized with TEA (Batch 2, 60±4 nm).

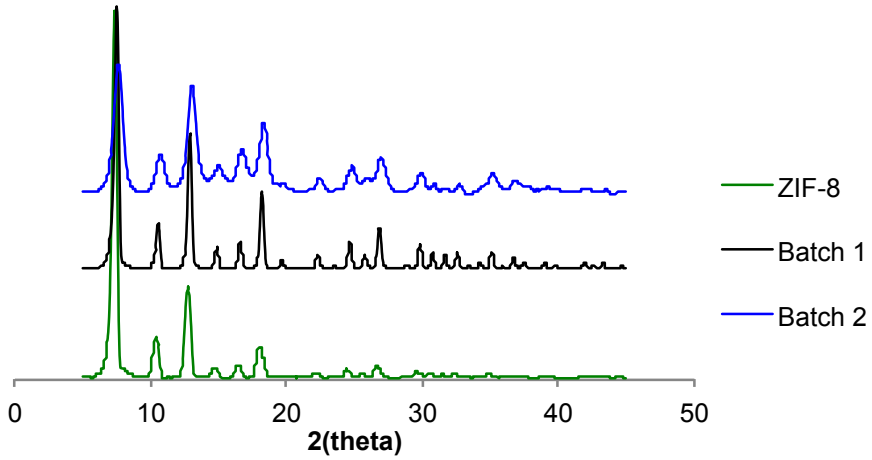

Figure 8. XRD patterns of synthesized ZIF-8 particles.

ZIF 20

ZIF-20 particles have an average diameter of 180 nm (Figure 9). The XRD pattern for this material is shown in Figure 10. At 160 °C, ZIF-20 underwent a color change (from white to orange). This was unexpected because a published TGA shows that the crystal does not decompose below 300 °C [3]. FTIR of ZIF-20 (not shown) before and after thermal treatment shows that the zinc-nitrogen bond (502 cm^{-1}) is intact. However, the carbonyl peak for DMF (1660 cm^{-1}) was present in the heated material, indicating that the solvent is trapped inside the ZIF cage, even after solvent exchange with methanol.

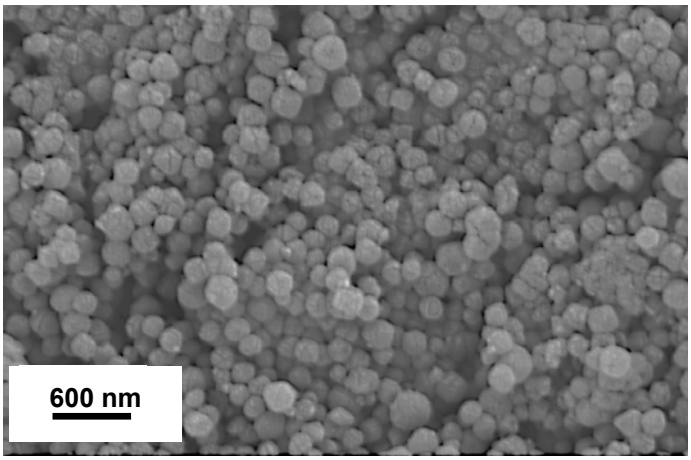

Figure 9. SEM image of ZIF-20 particles (average diameter = 180 nm)

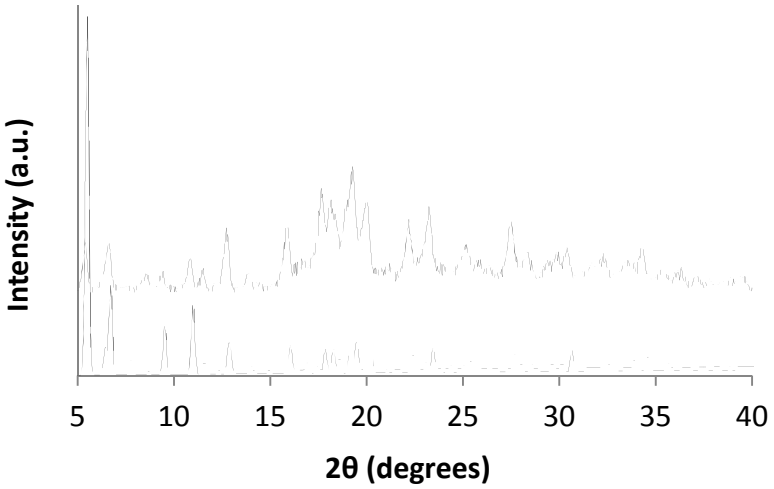

Figure 10. XRD patterns for ZIF-20: theoretical (bottom) and as-synthesized (top).

ZIF-90

The SEM image of synthesized ZIF-90 shows particles ~50 nm in diameter (Figure 11). XRD analysis shows that the material has the same reflections as the theoretical diffraction pattern (Figure 12). The thermal stability of ZIF-90 was observed to be greater than 300 °C (Figure 13), making it suitable for high temperature gas separations.

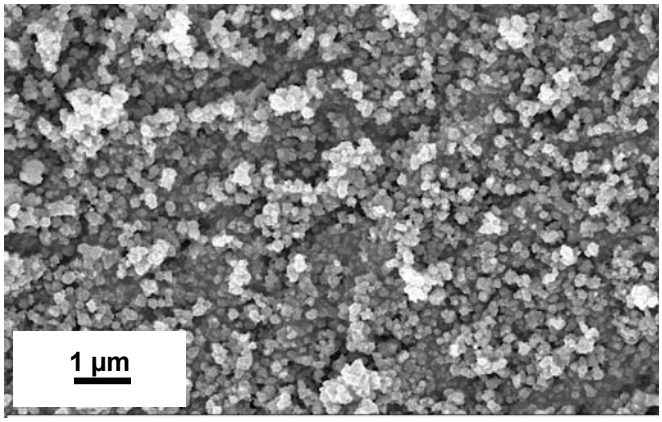

Figure 11. SEM image of synthesized ZIF-90 nanoparticles.

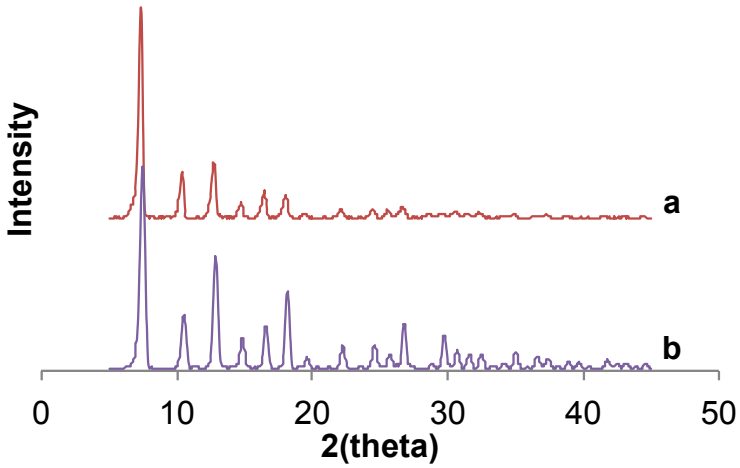

Figure 12. XRD patterns of ZIF-90: a) theroretical, b) synthesized nanoparticles (ZIF-90s).

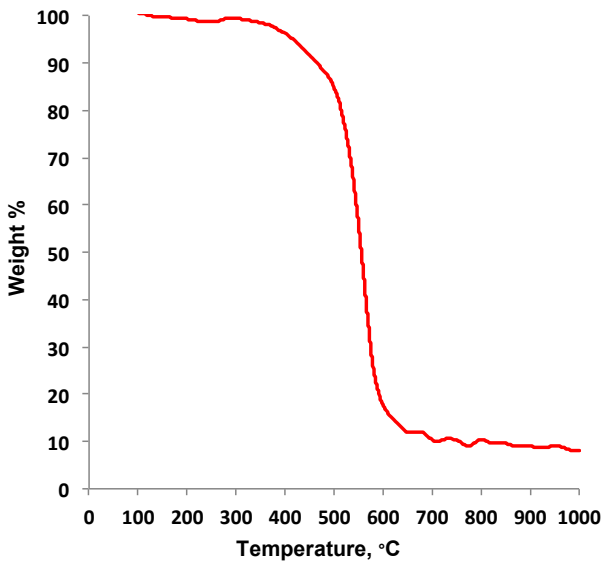

Figure 13. Thermogram of synthesized ZIF-90 nanoparticles.

ZIF 95

Sub-micron-sized particles of ZIF-95 (not shown) were synthesized by shortening the reaction time reported in the literature [19]. XRD revealed the correct XRD pattern (Figure 14).

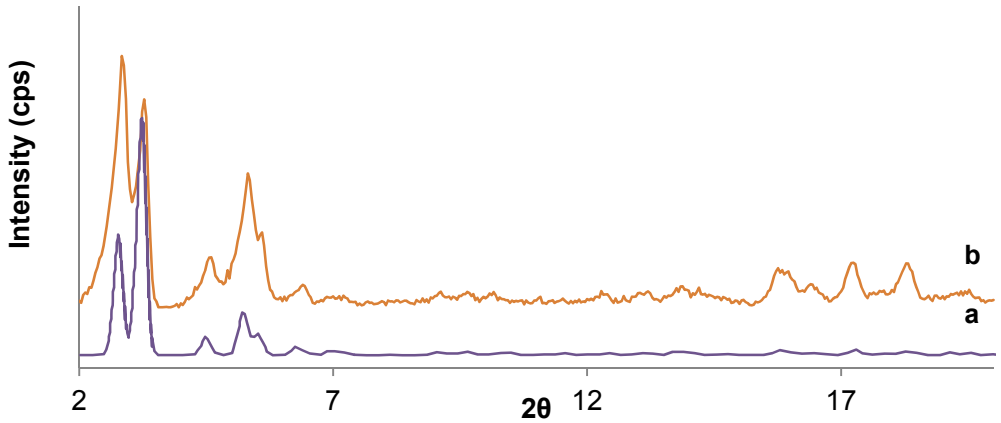

Figure 14. XRD patterns of ZIF-95: (a) theoretical [6] and (b) activated ZIF-95.

MIL-53 and NH_2-MIL-53

The optical and SEM images of NH_2-MIL-53 and MIL-53 powders, with Basolite® A100 as a comparison, are presented in Figure 15. All synthesized powders display nanometer-sized particles, comparable to the commercially available MIL-53.

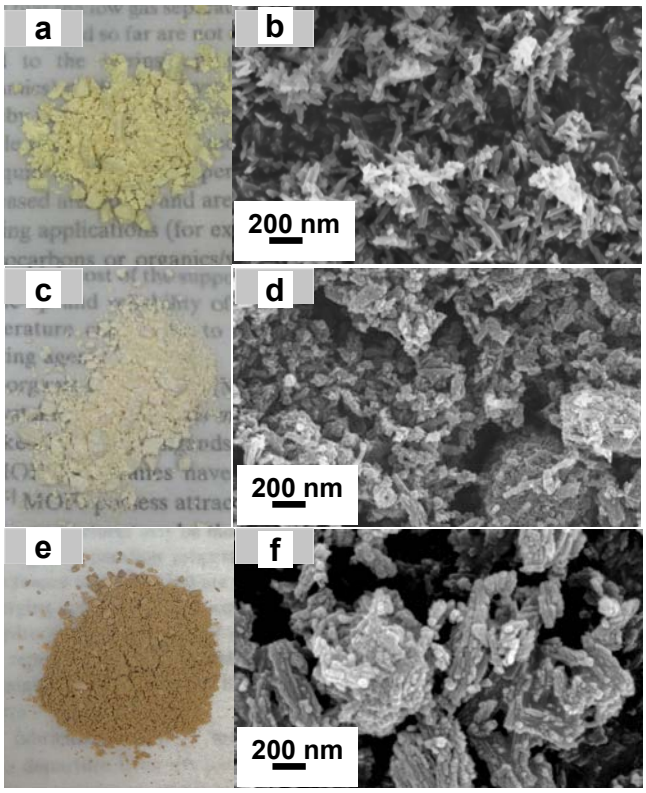

Figure 15. Optical (left) and SEM (right) images of NH_2-MIL-53 (a, b), MIL-53 (c, d), and Basolite® A100 (e, f).

X-ray diffraction patterns of MIL-53 acquired at temperatures up to 350 °C show that the material is thermally stable in the crystalline form (Figure 16). Also, the patterns show that, depending on temperature, the material exists in either an open pore form (MIL-53-ht), or a mixed open pore/closed pore (MIL-53-lt) form.

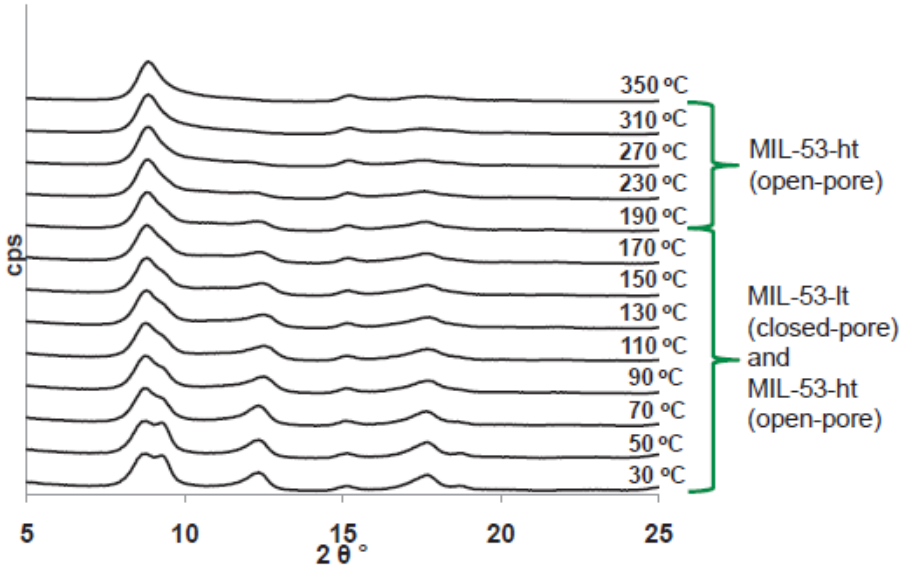

Figure 16. Temperature-dependent XRD patterns of MIL-53.

N_2 absorption-desorption type I isotherms of MIL-53-ht and MIL-53-lt indicate that both materials are microporous (Figure 17). BET surface areas of 1118 m^2/g and 900 m^2/g were determined from the isotherms of MIL-53-ht and MIL-53-lt, respectively. The Langmuir surface areas reported for MIL-53(Cr) are estimated to be over 1500 and 1150 m^2/g, respectively [20], which are close to those obtained for MIL-53(Al).

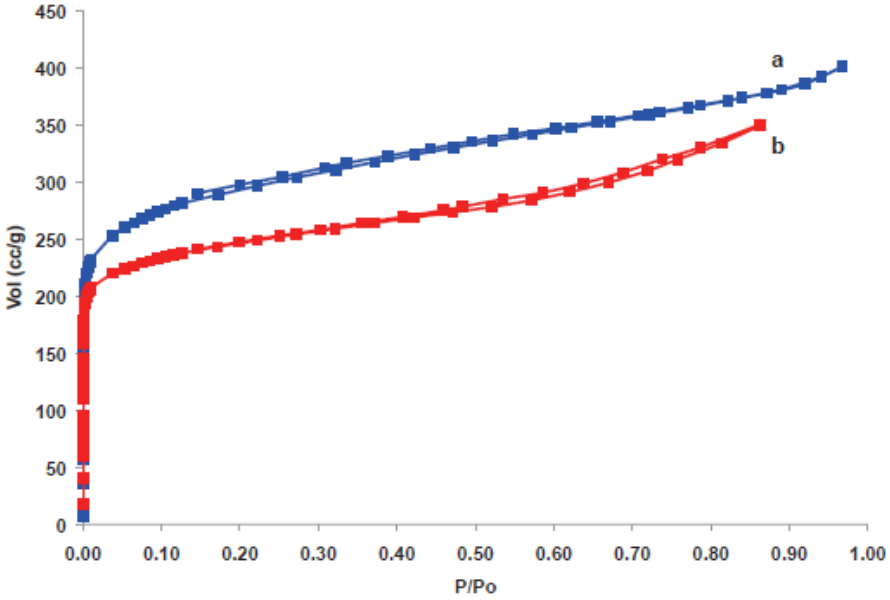

Figure 17. N_2 adsorption-desorption isotherms of a) MIL-53-ht and b) MIL-53-lt.

MOP-18

XRD patterns of MOP-18 simulated from experimental single-crystal X-ray data (Figure 18a) [9] and of synthesized MOP-18 particles (Figure 18 b,c) are shown below. The position of the main reflection for the material recrystallized from methanol is shifted 0.5° to a higher angle indicating a contraction of the unit cell. When recrystallized from a hexane/heptanol mixture, the XRD pattern (Figure 18c) matches the theoretical pattern confirming that the material is MOP-18 [9].

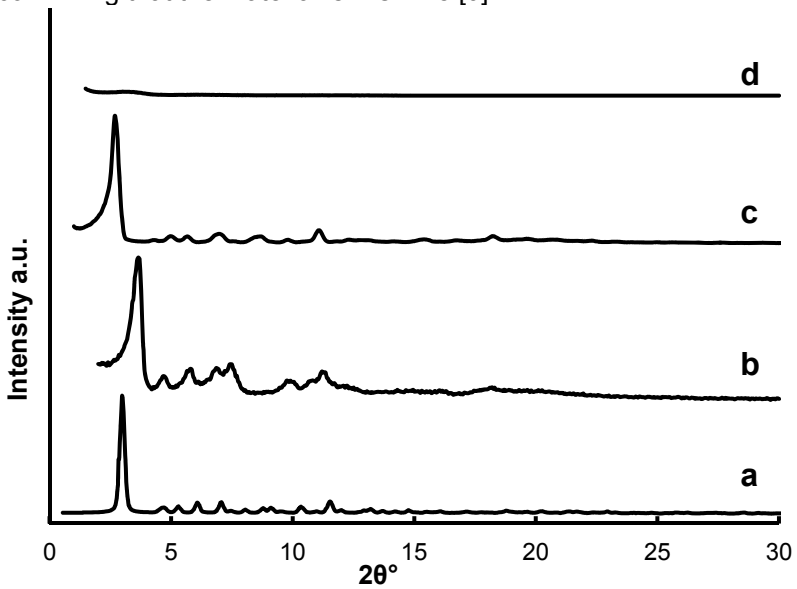

Figure 18. XRD patterns of MOP-18: a) theoretical, b) experimental, recrystallized from methanol, c) experimental, recrystallized from hexanes/heptanol, and d) 80% (w/w) MOP-18/Matrimid® membrane.

Mixed-matrix membranes

ZIF-7/Matrimid® MMMs

Figure 19 shows a SEM image of a cross-section of a 20% (w/w) ZIF-7/Matrimid® MMM. The ZIF-7 nanocrystals appear to be well dispersed within the polymer matrix, suggesting a good interface between the ZIF-7 nanocrystals and Matrimid®. More importantly, there was no indication that non-selective voids were present in the matrix.

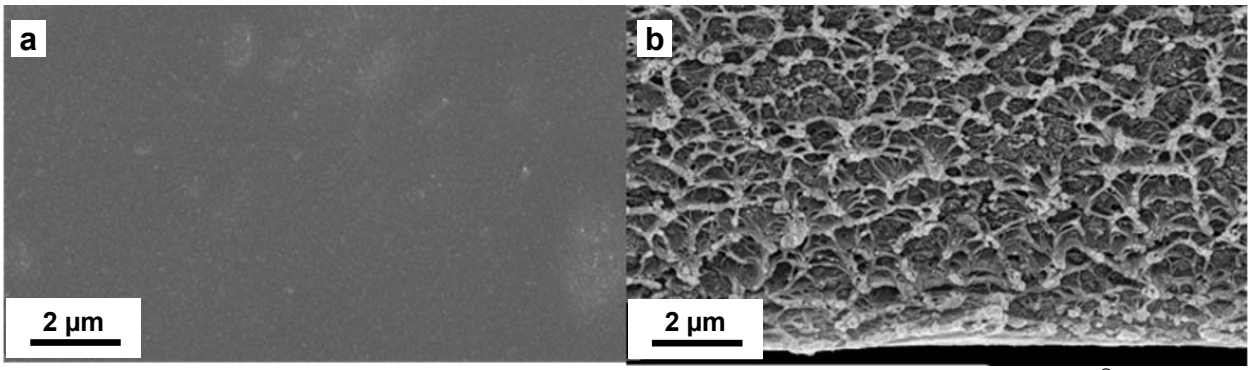

Figure 19. SEM images of surface (a) and cross-section (b) of 20% (w/w) ZIF-7/Matrimid® MMM.

Gas permeation measurements revealed that the MMM was less permeable for all gases tested than pure Matrimid® (Table 1). The permeability data at this loading suggests that ZIF-7 acts as a filler. While the gas selectivity values were generally lower for the MMM than for pure Matrimid® (Table 2), the values were well above Knudsen selectivity, suggesting that the membrane remained structurally sound during the permeability experiments.

Compared to the 20% (w/w) loading, hydrogen and carbon dioxide permeability were higher for a 30% (w/w) ZIF-7/Matrimid® MMM and the membrane remained selective. However, high permeability values for nitrogen and methane suggest that nonselective voids may have been present in the membrane (Tables 1 and 2).

Table 1. Permeability data for 20% and 30% (w/w) ZIF-7/Matrimid® MMMs annealed at 100 °C

Gas	20% (w/w) MMM	30% (w/w) MMM	Matrimid®
N_2	0.18 ± 0.05	2285 ± 66.5	0.24
O_2	1.2 ± 0.34	1639 ± 272.4	1.49
CH_4	0.13 ± 0.03	3524 ± 39.9	0.22
CO_2	5.6 ± 0.76	889.7 ± 61.2	7.33
H_2	16.5 ± 8.10	2368 ± 200.6	17.08

Table 2. Selectivity data for 20% and 30% (w/w) ZIF-7/Matrimid® MMMs annealed at 100 °C

Gas	20% (w/w) MMM	30% (w/w) MMM	Matrimid®	Knudsen Diffusion
H_2/O_2	13.7 ± 2.99	1.44	11.46	4.00
H_2/CO_2	2.95 ± 1.05	2.66	2.33	4.70
H_2/N_2	91.6 ± 40.1	1.04	70.32	3.74
H_2/CH_4	126 ± 47.9	0.67	76.62	2.82

ZIF-8/Matrimid® MMMs [18]

The SEM image of a 50% (w/w) ZIF-8/Matrimid® MMM cross-section shows uniform dispersion of the ZIF-8 material in the polymer matrix (Figure 20). The presence of the concentric cavities in the MMM indicates that there is a strong interfacial contact between Matrimid® and the ZIF-8 nanoparticles.

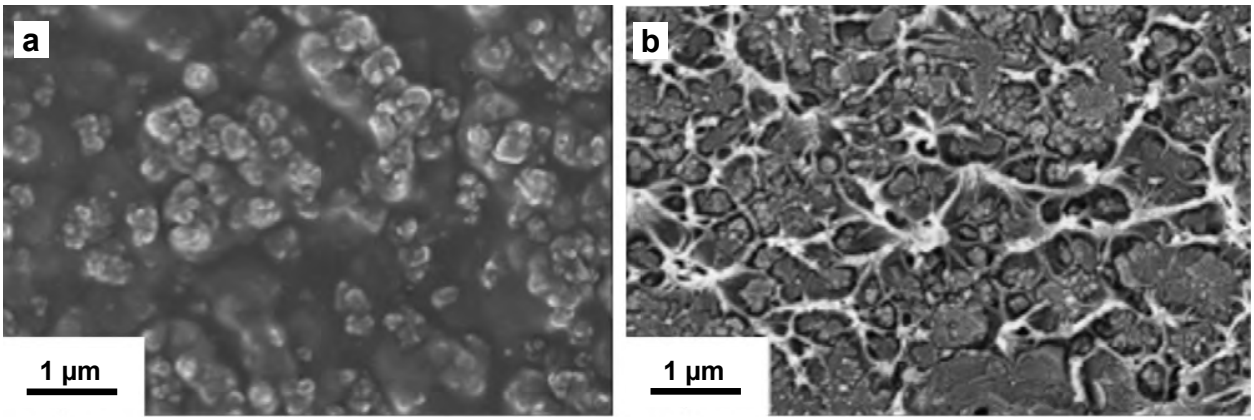

Figure 20. SEM images of air-surface (a) and cross-section (b) of a 50% (w/w) ZIF-8/Matrimid® MMM.

The permeability values (Figure 21) obtained for all gases tested increased as the ZIF-8 loading increased up to 40% (w/w). However, at higher loadings of 50% and 60% (w/w), the permeability decreased for all gases. This result suggests a transition from a polymer-driven to a ZIF-8-controlled gas transport process, where at higher loadings the sieving effect of the ZIF-8 nanocrystals is more evident. Increases in ideal selectivities (Figure 22) were obtained at the higher ZIF-8 loadings for gas pairs containing small gas molecules, such as H_2/O_2 and CO_2/C_3H_8, suggesting that the ZIF-8 may act as a molecular sieve for smaller gas molecules [18].

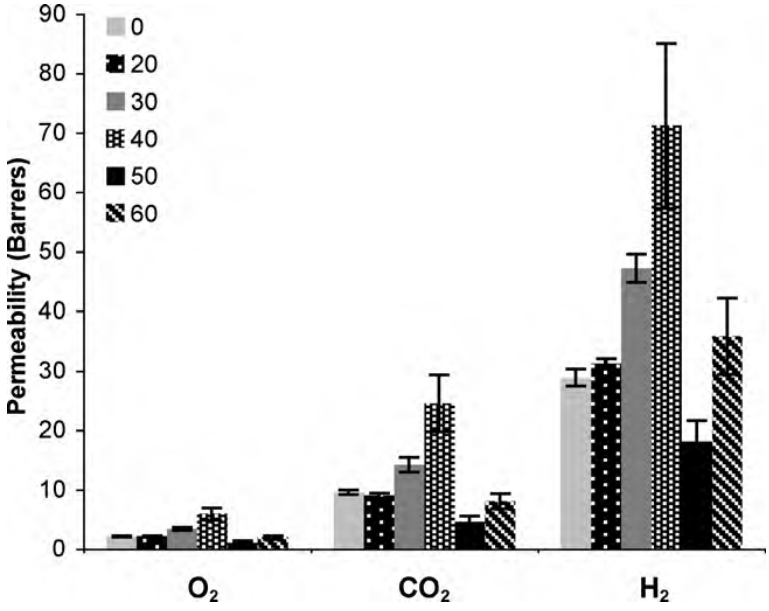

Figure 21. Plot of permeability versus loading for O_2, CO_2, and H_2 at 0%, 20%, 30%, 40%, 50%, and 60% (w/w) ZIF-8 loadings [18].

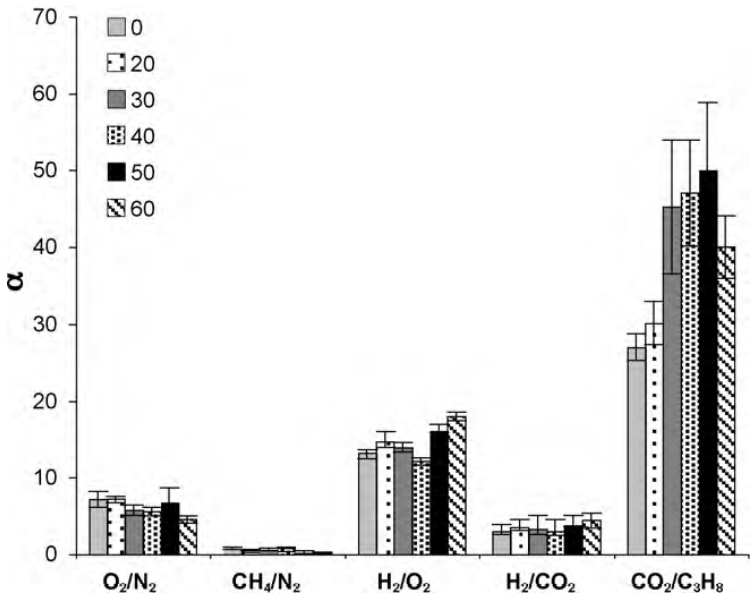

Figure 22. Ideal selectivity plots of ZIF-8/Matrimid® MMMs for O_2/N_2, CH_4/N_2, H_2/O_2, H_2/CO_2, and CO_2/C_3H_8 at 0%, 20%, 30%, 40%, 50%, and 60% (w/w) ZIF-8 loadings [18].

EDA cross-linked ZIF-8/Matrimid® and EDA cross-linked, spin-coated Matrimid® ZIF-8/Matrimid® MMMs

Figure 23 shows SEM images of EDA cross-linked ZIF-8/Matrimid® MMMs. When compared to Matrimid®, a decrease in gas permeabilities for EDA cross-linked Matrimid® was observed for all gases tested (Figure 24). Permeabilities decreased by 52% for H_2, 95% for CO_2, 89% for O_2, 75% for N_2, and 73% for CH_4. The decrease in permeabilities can be attributed to the presence of densified polymer chains. However, the permeabilities increased for both the EDA cross-linked 40% and 50% (w/w) ZIF-8/Matrimid® MMMs compared to the 40% and 50% (w/w) ZIF-8/Matrimid® MMMs. The cross-linked 40% (w/w) ZIF-8/Matrimid® MMM exhibited an increase in permeabilities of 152% for H_2, 122% for CO_2, 170% for O_2, 495% for N_2, and 15% for CH_4, while the cross-linked 50% (w/w) ZIF-8/Matrimid® MMM increased 340% for H_2, 274% for CO_2, 186% for O_2, 959% for N_2, and 84% for CH_4. The increase in permeabilities could be due to the delamination of ZIF-8 as a consequence of the dissolution of Matrimid® upon long exposure to EDA vapor. This would weaken the polymer-MOF interface creating voids or defects on the surface of the MMM resulting in increased permeabilities of the penetrant gases.

The selectivity plots in Figure 25 show an increase in selectivity for hydrogen-containing gas pairs including H_2/CO_2, H_2/O_2, H_2/CH_4 and H_2/N_2 for the EDA cross-linked Matrimid® compared to Matrimid®. The increase in the selectivities of the EDA cross-linked Matrimid® membranes can be attributed to the cross-linking of the diffusive pathways for gases such as CO_2. This increase in selectivity suggests that there was a reduction in the diffusive pathways for the larger gas molecules compared to the smaller H_2 molecule. For the cross-linked ZIF-8/Matrimid® MMMs, the selectivities of some gas pairs are close to Knudsen selectivity values, which could be due to defects in the MMMs brought about by cross-linking. However, compared to the uncross-linked MMMs, the H_2/CO_2 selectivity stayed the same for both loadings of the cross-linked ZIF-8/Matrimid® MMMs, and thus the separation of H_2 and CO_2 remains challenging due to the trade-off between H_2/CO_2 solubility selectivity and diffusivity selectivity.

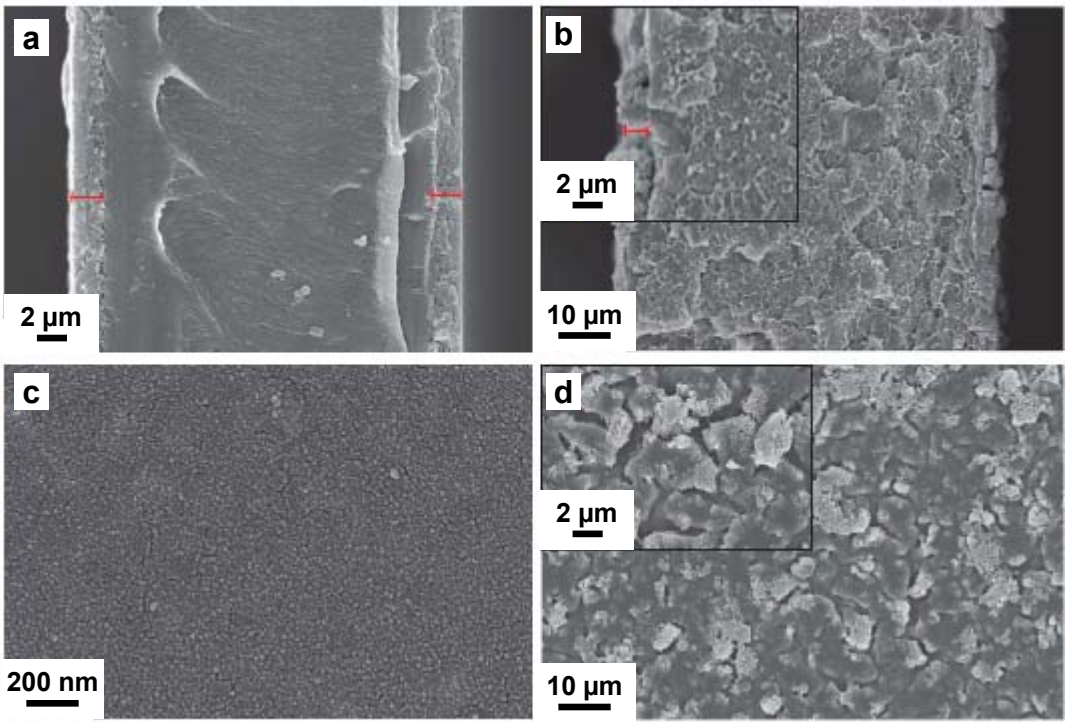

Figure 23. SEM images of the cross-sections (top) and surface (bottom) of (a) & (c) a Matrimid® membrane and (b) & (d) a ZIF-8/Matrimid® MMM both cross-linked with EDA vapor. The cross-linked layers are noted by the red bars in (a) & (c).

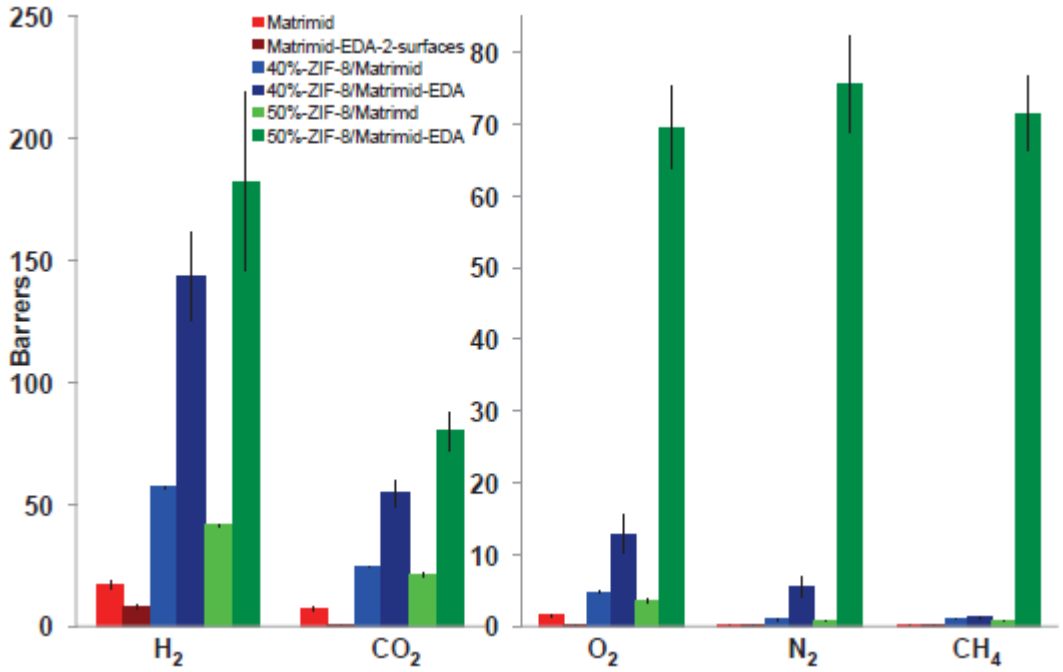

Figure 24. Permeability plots for ZIF-8/Matrimid® MMMs cross-linked with EDA vapor.

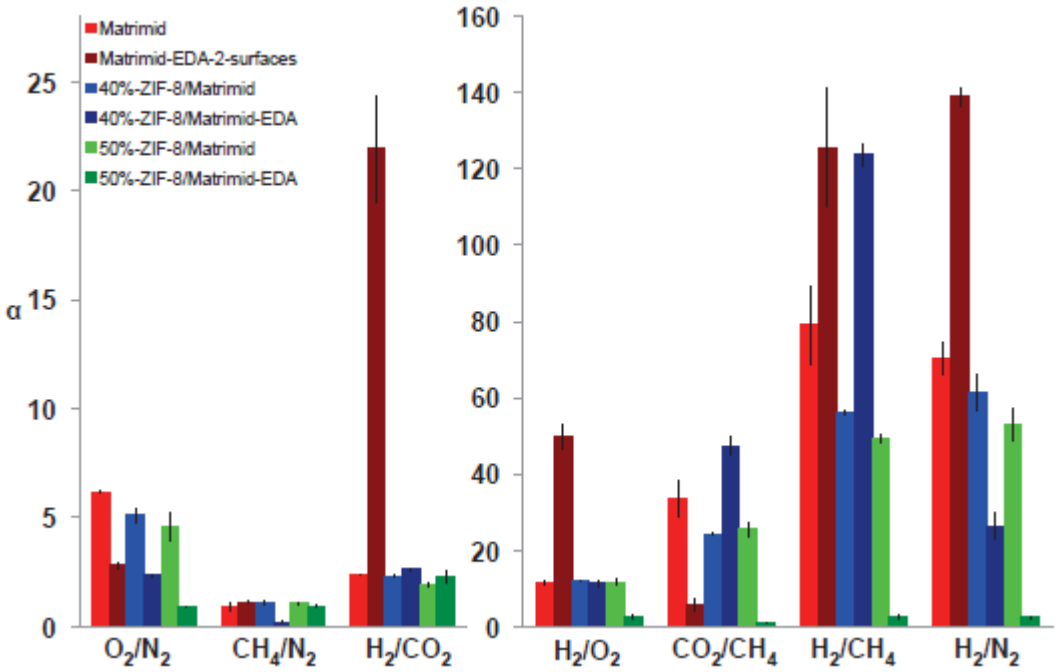

Figure 25. Selectivity plots for ZIF-8/Matrimid® MMMs cross-linked with EDA vapor.

Figure 26 shows an SEM image of 40% and 50% (w/w) ZIF-8/Matrimid® MMMs with an EDA cross-linked Matrimid® layer of 1.8 µm. The permeabilities (Figure 27) for all gases decreased for the cross-linked, spin-coated Matrimid® 40% and 50% (w/w) ZIF-8/Matrimid® MMMs compared to their corresponding uncross-linked MMMs. The cross-linking provided a densified polymer component rendering the slower diffusion of gas molecules and, consequently, resulting in a decrease in the gas permeabilities of the membranes. Another factor that may contribute to the observed decrease in permeabilities is the

blockage of ZIF-8 pores at the interface of the cross-linked, spin-coated Matrimid® layer. Compared to the 40% and 50% (w/w) ZIF-8/Matrimid® MMMs, increases in selectivities were measured for both the cross-linked, spin-coated Matrimid® 40% and 50% (w/w) ZIF-8/Matrimid® MMMs for H_2/CO_2, H_2/O_2, H_2/CH_4, and H_2/N_2 gas pairs (Figure 28). The increase in the ideal selectivities for these gas pairs is most probably the result of an increase in diffusivity selectivity because smaller molecules, like H_2, could more easily penetrate the less accessible cross-linked structure (lower fractional free volume) than larger molecules like N_2, O_2, and CH_4. In these gas pairs, the H_2 gas molecules have a small kinetic diameter (H_2: 2.89 Å; CO_2: 3.3 Å; O_2: 3.46 Å; N_2: 3.64 Å; CH_4: 3.8 Å) and can diffuse faster as compared to nitrogen, oxygen, and methane gases that are bigger and quite soluble (critical temperature: H_2: 32.97; CO_2: 87.98; O_2: 154.6; N_2: 190.56; CH_4: 304.13) in the polymer.

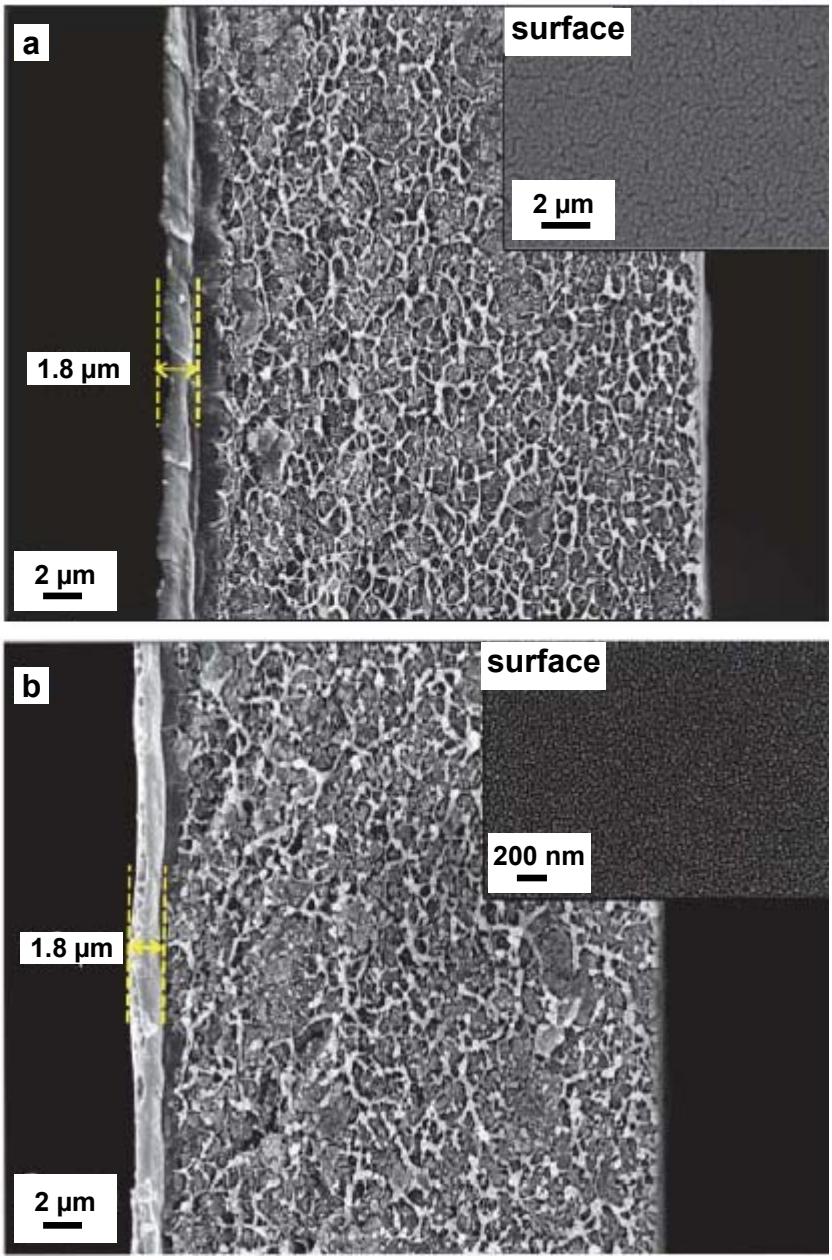

Figure 26. SEM images of cross-sections and surfaces of a) 40% (w/w) and b) 50% (w/w) ZIF-8/Matrimid® MMMs that were spin-coated on one surface with Matrimid® and cross-linked with EDA.

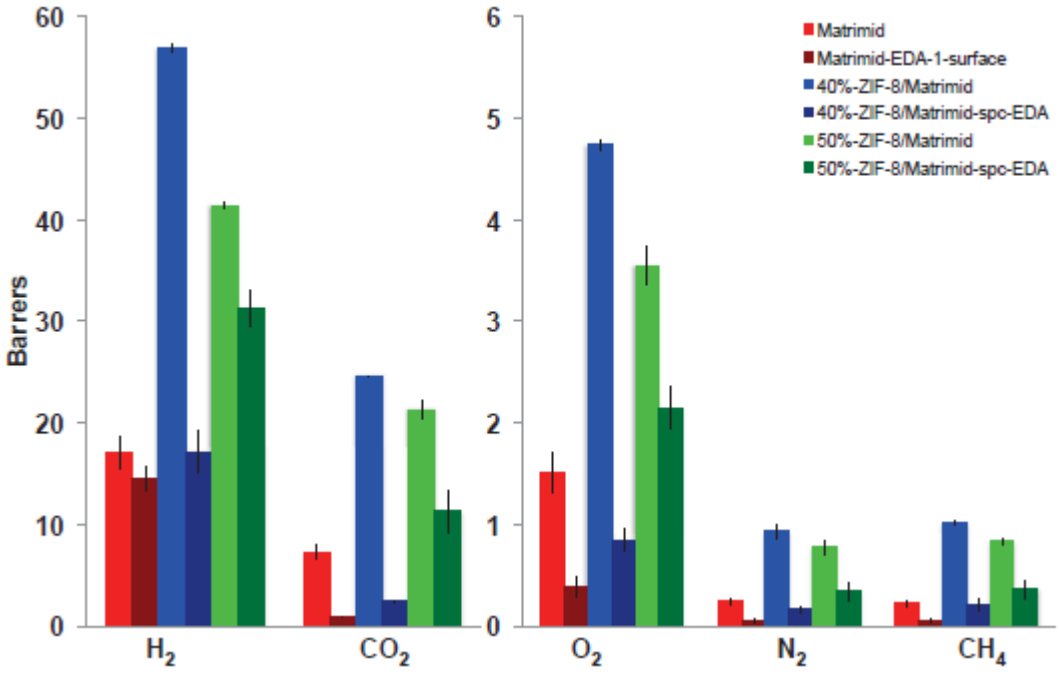

Figure 27. Permeability plot for EDA cross-linked, spin-coated Matrimid® ZIF-8/Matrimid® MMMs.

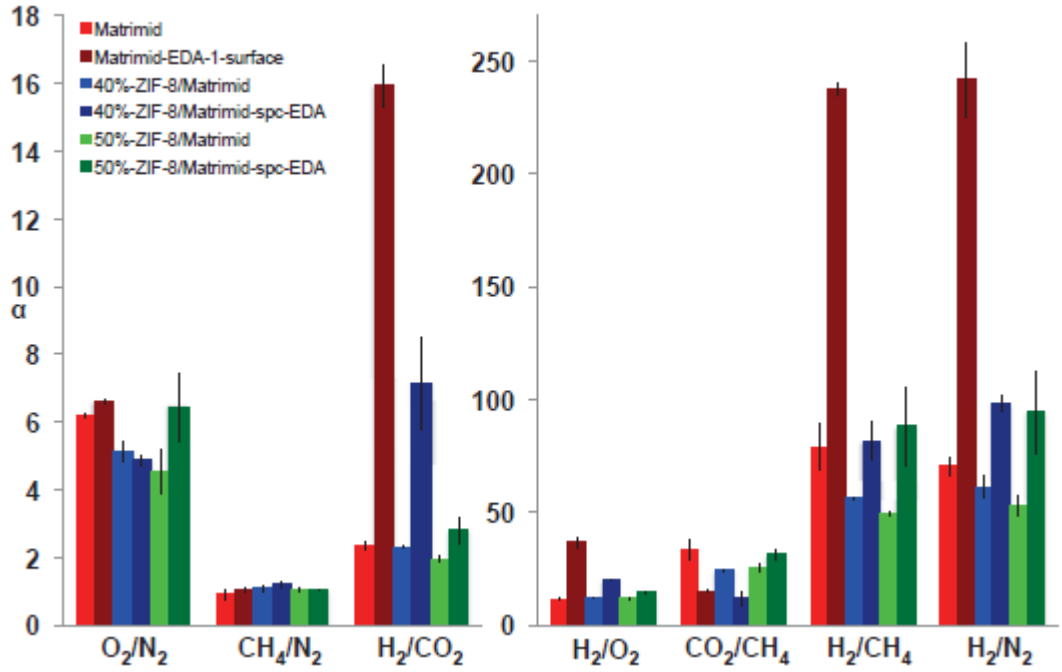

Figure 28. Selectivity plot for EDA cross-linked, spin-coated Matrimid® ZIF-8/Matrimid® MMMs.

MIL-53/Matrimid® MMMs

SEM images (Figure 29) of a 50% (w/w) MIL-53-lt/Matrimid® MMM cross-section showed that there was good dispersion of the MIL-53-lt additive in the MMM and that no major defects were present at this magnification.

The MIL-53-ht/Matrimid® and MIL-53-as/Matrimid® MMMs exhibited higher values of permeability compared to Matrimid® (Figure 30) as well as increases in CO_2/CH_4 selectivity (Figure 31) suggesting that the open-pore MIL-53 framework was maintained in the polymer matrix.

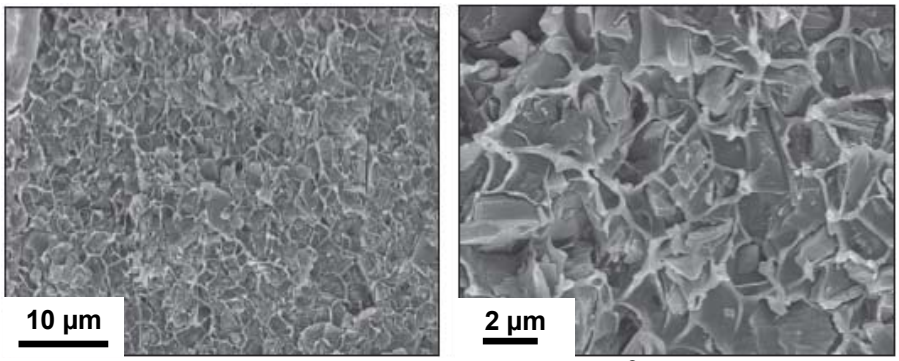

Figure 29. SEM images of 50% (w/w) MIL-53-lt/Matrimid® MMM cross-sections.

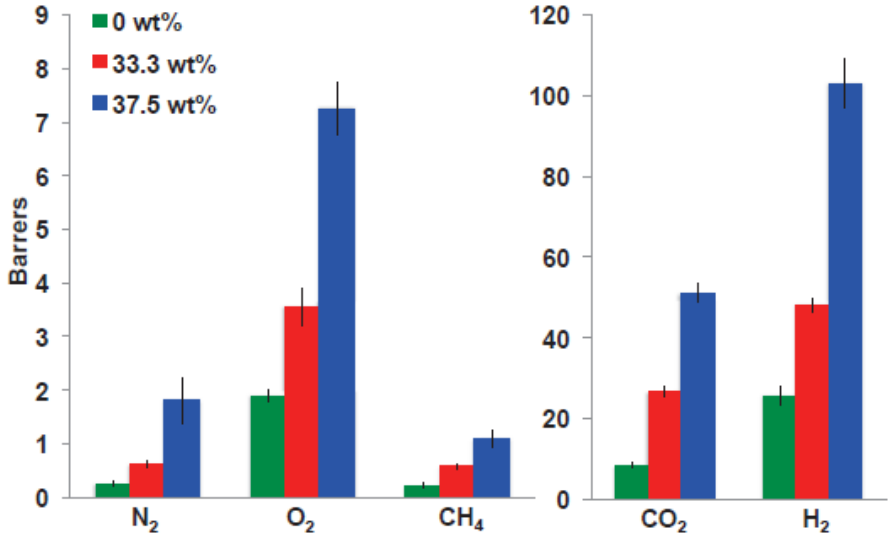

Figure 30. Permeability plots of 50% (w/w) and 60% (w/w) MIL-53-ht/Matrimid® MMMs.

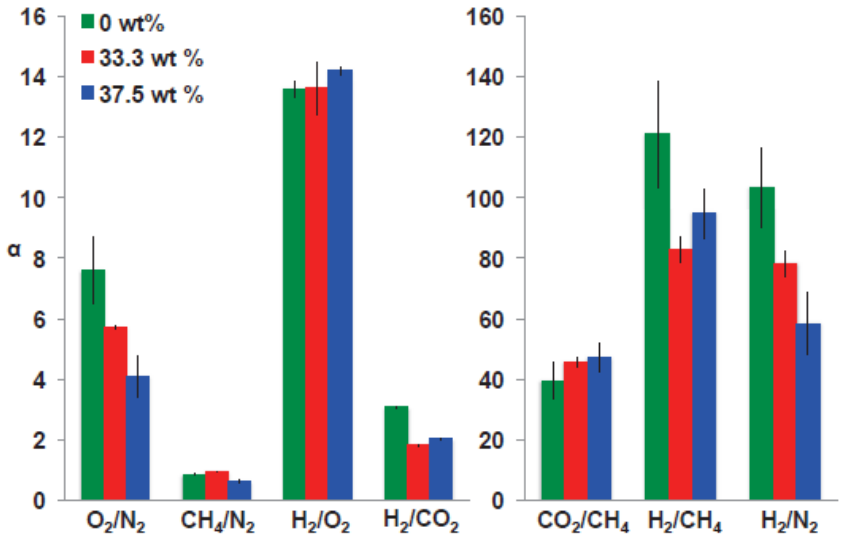

Figure 31. Selectivity plots of 50% (w/w) and 60% (w/w) MIL-53-ht/Matrimid® MMMs.

PIM-1-based MMMs

The molecular weight of the synthesized PIM-1 as measured by GPC was 126 kDa with a PDI of 2.7. The thin and flexible PIM-1 film that was prepared by casting in chloroform is shown in Figure 32.

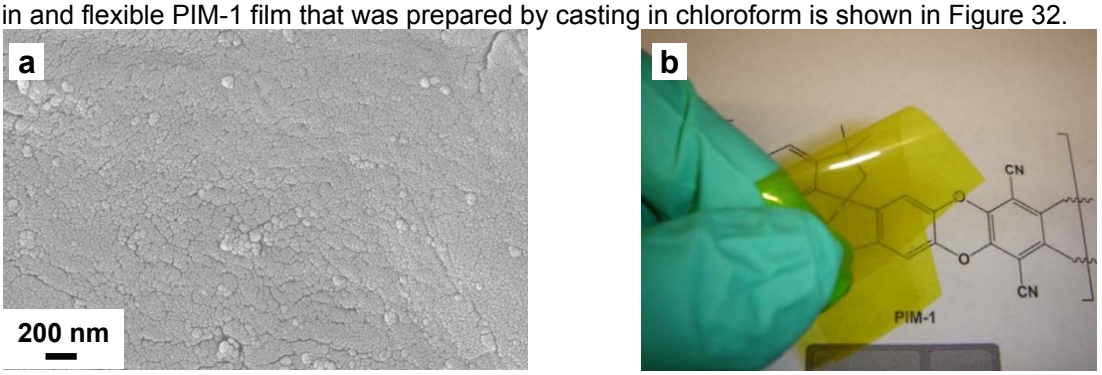

Figure 32. Images of a PIM-1 membrane: (a) SEM image of cross-section, and (b) optical image of film.

Metal-organic framework nanoparticles (ZIF-8, ZIF-90, MIL-53) were incorporated into PIM-1 at weight loadings up to 17.6% (w/w) (Figure 33). The 11.1% (w/w) ZIF-90/PIM-1 MMM is transparent at this loading due to the good dispersion of the nanosized ZIF-90 particles (Figure 33C). The ZIF-8 and MIL-53 MMMs retained the crystallinity of the MOFs even after annealing at 300 °C for 2 d (Figures 34A and B). Preliminary permeability results of the ZIF-8/PIM-1 and MIL-53/PIM-1 MMMs (annealed at 300 °C) show increased permeabilities for all gases tested (H_2 permeabilities increased at least 20x when compared to a pure PIM-1 film), but without any significant improvement in selectivities. These results also show that the thermal treatment applied to PIM-1 films greatly affects their permeability properties.

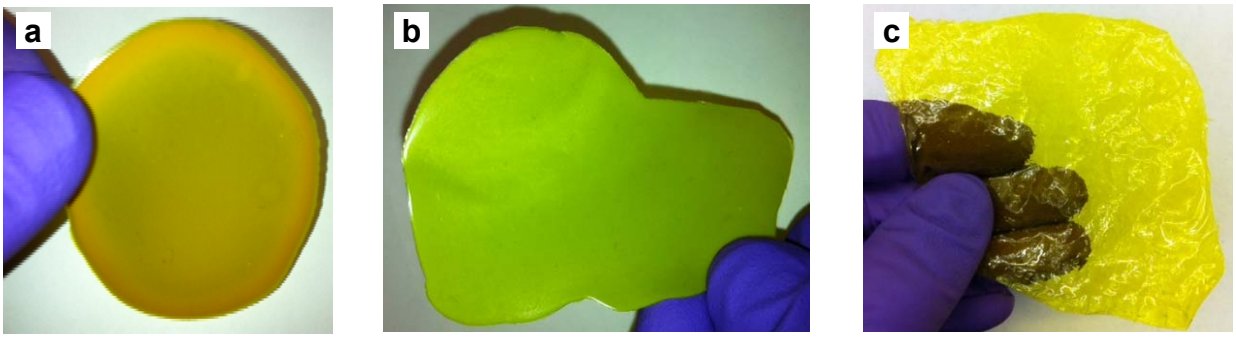

Figure 33. Photographs of PIM-1-based MMMs, (a) 11.1% (w/w) MIL-53/PIM-1 MMM, (b) 17.6% (w/w) ZIF-8/PIM-1 MMM, and (c) 11.1% (w/w) ZIF-90 ZIF-90/PIM-1.

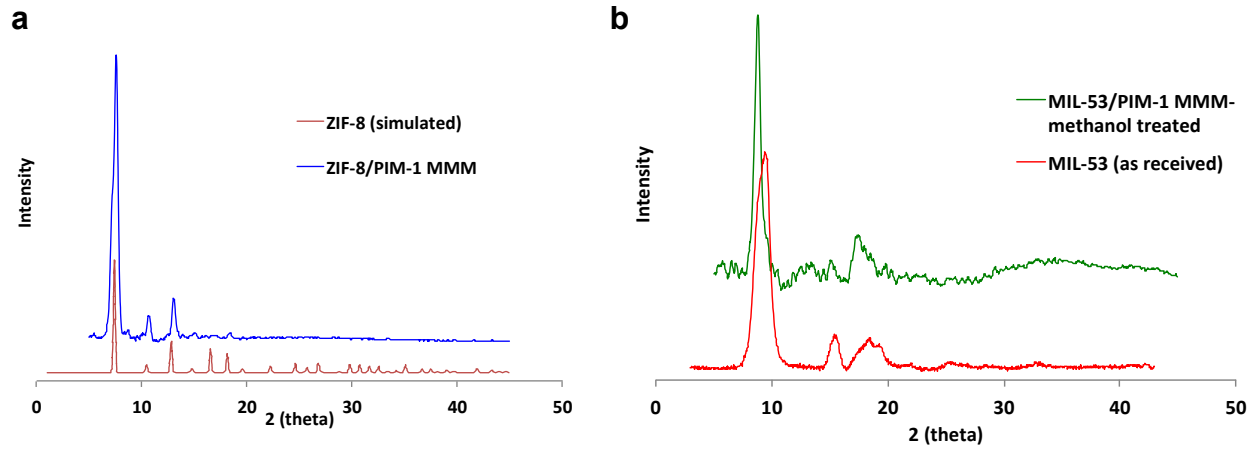

Figure 34. XRD patterns of PIM-1 based MMMs after methanol treatment and annealing at 300 °C for 2 d: (a) 17.6% (w/w) ZIF-8/PIM-1 MMM, and (b) 11.1% (w/w) MIL-53/PIM-1 MMM.

6FDA-ODA/NDA-based MMMs

Five polyimide (PI) polymers (6FDA-NDA, 6FDA-ODA, and their copolymers (3:1, 1:1, 1:3 molar ratios)) were synthesized with high molecular weights (Table 3) following published procedures.

Table 3. Molecular weights of synthesized polyimides as measured by GPC

Polymer	M_w, Da	M_n	PDI
6FDA-NDA	71000	31840	2.23
6FDA-ODA	60000	25860	2.32
6FDA-NDA-ODA (3:1)	70000	29166	2.40
6FDA-NDA-ODA (1:1)	89000	31700	2.80
6FDA-NDA-ODA (1:3)	80000	25000	3.20

These polymers were selected due to their thermal stabilities (Figure 35) up to temperatures of 480 °C and their T_g's at least 300 °C (Table 4).

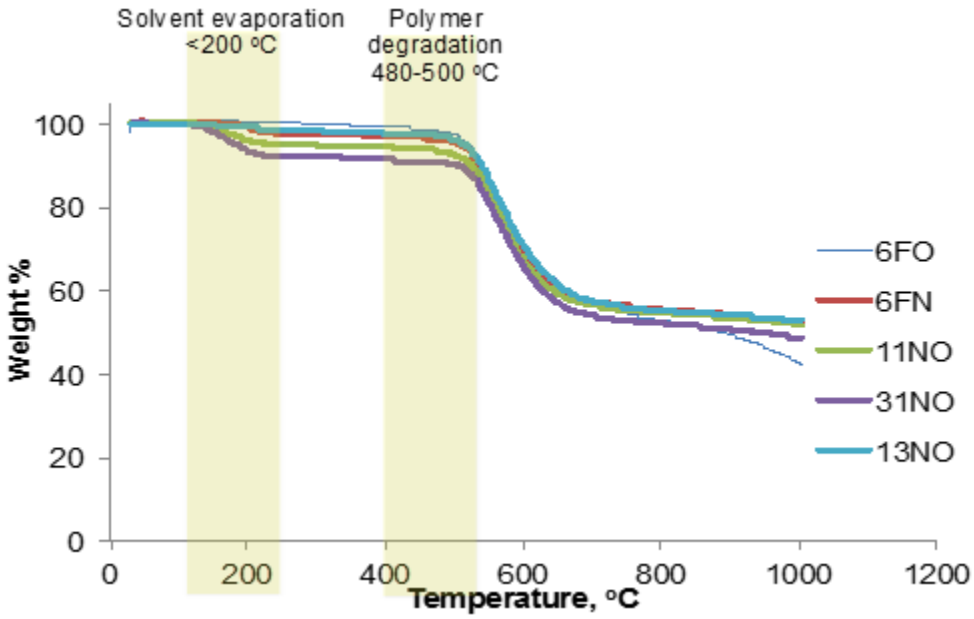

Figure 35. Thermograms of synthesized PIs.

Table 4. Thermal properties of synthesized PIs

Polymer	T_d at 10%, °C	T_g, °C
6FDA-NDA	480	394
6FDA-ODA	480	304
6FDA-NDA-ODA (3:1)	480	350
6FDA-NDA-ODA (1:1)	480	337
6FDA-NDA-ODA (1:3)	480	325

The PI polymers were prepared as films by dissolving in DMF or chloroform and casting onto glass substrates. Thin and flexible films were characterized by SEM (Figure 36). The textured morphology observed for the 6FDA-NDA polymer at the 200 nm scale is characteristic of polyimide membranes (Figure 36). Several MMMs with these PIs as polymer matrix were prepared and the results will be discussed in the following sections.

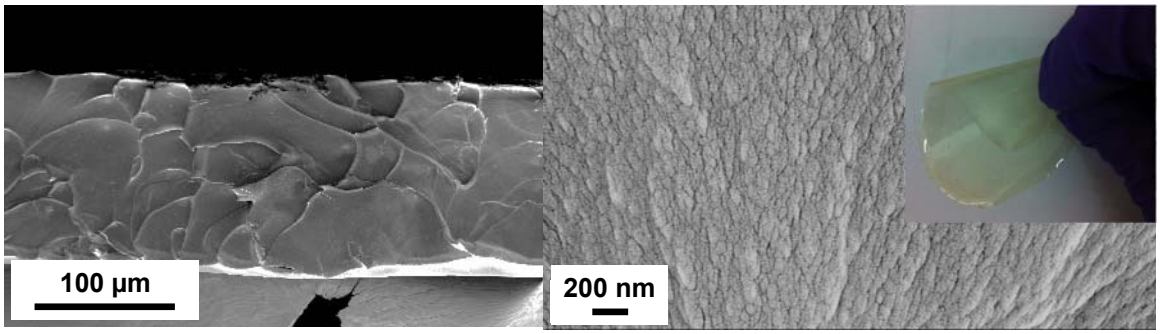

Figure 36. SEM images of 6FDA-NDA polymer cross-section. Insert shows the optical image of a 6FDA-NDA film.

MMMs were prepared comprising the PI polymers and ZIFs or MOFs. MMMs of 25% (w/w) ZIF-8/6FDA-NDA were fabricated using ZIF-8 of different particle sizes including commercially available ZIF-8 (Basolite® Z1200, 120 nm particles) and synthesized ZIF-8 (111 nm and 60 nm particle sizes) (Figure 37). It was expected that the smallest particles would disperse best in the polymers. Improved polymer wetting of ZIF-8 was observed for the smallest 60 nm particles, but severe aggregation was also present. To overcome this aggregation, colloidal ZIF-8 particles were prepared and used for MMM fabrication. The use of a colloidal ZIF synthesis solution directly for MMM fabrication (without drying the particles) led to transparent MMMs and better dispersion (as shown by the SEM images) at the same ZIF-8 loading (Figure 38). Due to the small size of the ZIF-8 particles, it was challenging to identify what was ZIF or polymer nodules in the SEM images.

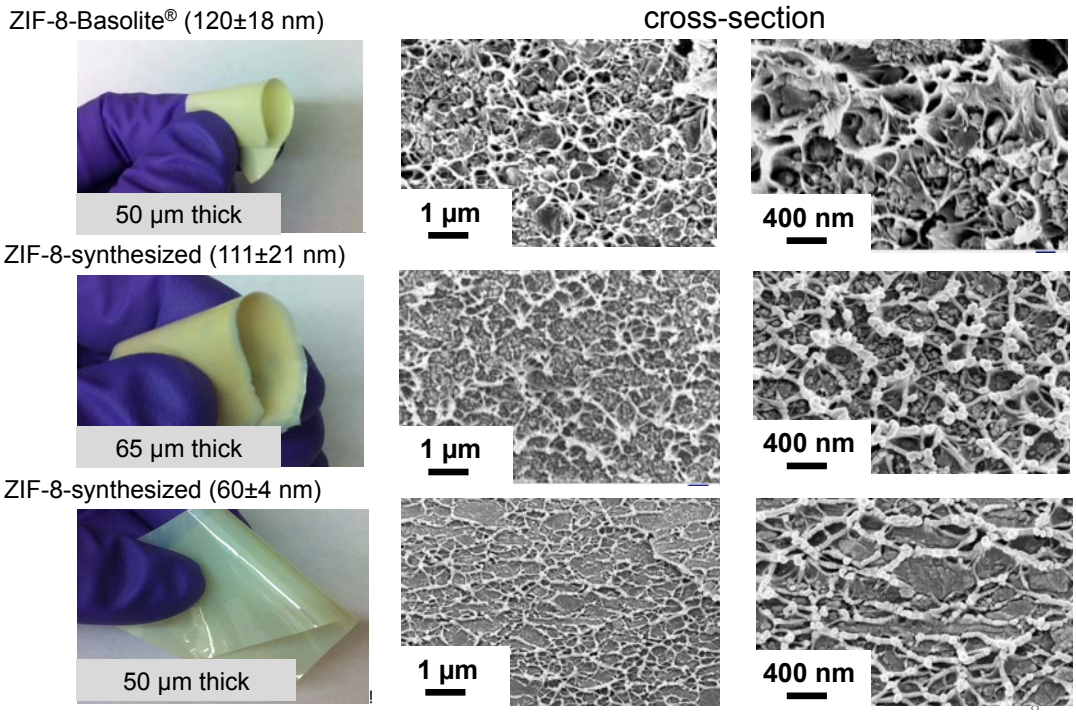

Figure 37. Optical and SEM images of 25% (w/w) ZIF-8/6FDA-NDA MMMs prepared using ZIF-8 with different particle sizes.

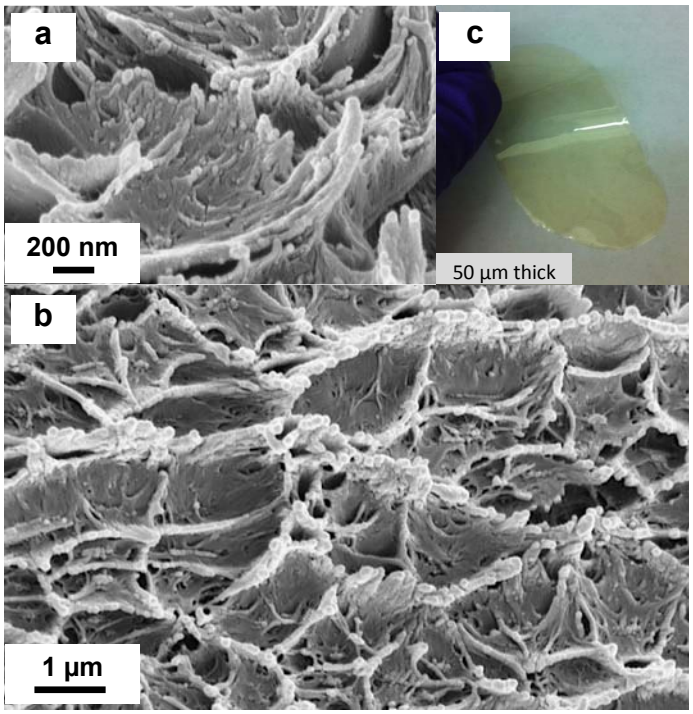

Figure 38. (a,b) SEM images and (c) optical image of a 25% (w/w) colloidal ZIF-8/6FDA-NDA MMM.

The use of colloidal ZIF solutions for MMM fabrication was extended to ZIF-7/PI MMMs. A 25% (w/w) ZIF-7/6FDA-NDA MMM was fabricated to form a transparent and flexible film (Figure 39). The loading of the ZIF-7 in 6FDA-NDA was increased to 100% (w/w) (Figure 40), and the resulting film was still transparent. XRD patterns of the MMMs show that ZIF-7 particles (not necessarily all) are intact in the polymer (Figure 41). However, at ZIF-7 loadings higher than 25% (w/w) the MMMs become brittle. To provide better interaction between polymer and ZIF without lowering the thermal stability of the polymer, a 3:1 mol ratio 6FDA-NDA-ODA copolymer (T_g = 350 ºC, Table 10) was used as the polymer matrix for ZIF-7 (Figure 42). Similar to the other MMMs with ZIF-7, the 25% (w/w) ZIF-7/6FDA-NDA-ODA (3:1) MMM was also transparent.

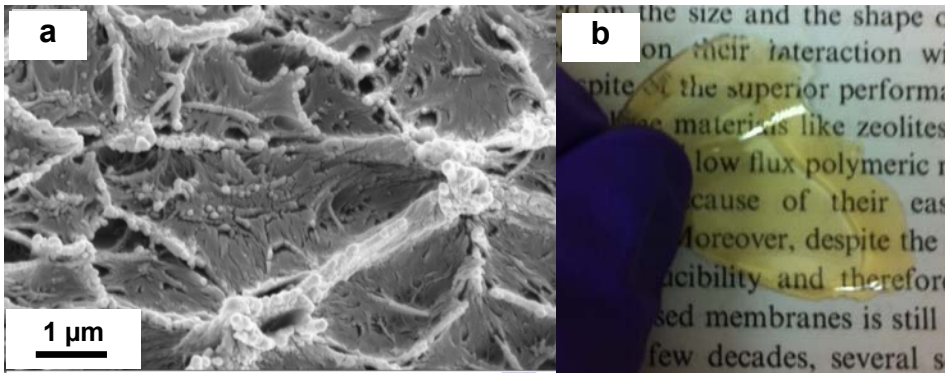

Figure 39. (a) SEM image of MMM cross-section, and (b) optical image of a 25% (w/w) ZIF-7/6FDA-NDA MMM.

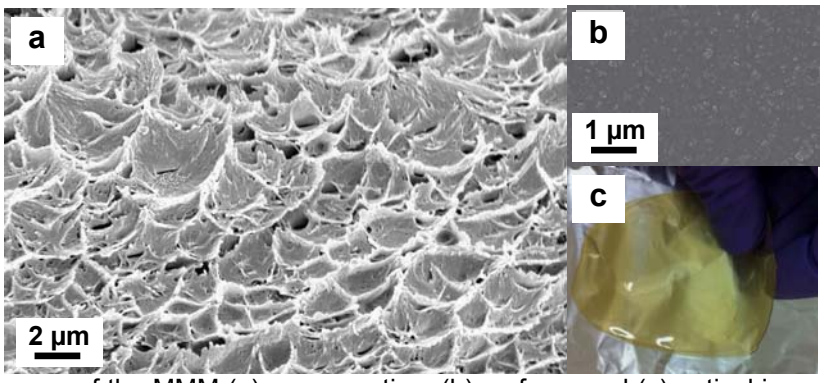

Figure 40. SEM images of the MMM (a) cross-section, (b) surface, and (c) optical image of a 100% (w/w) ZIF-7/6FDA-NDA MMM.

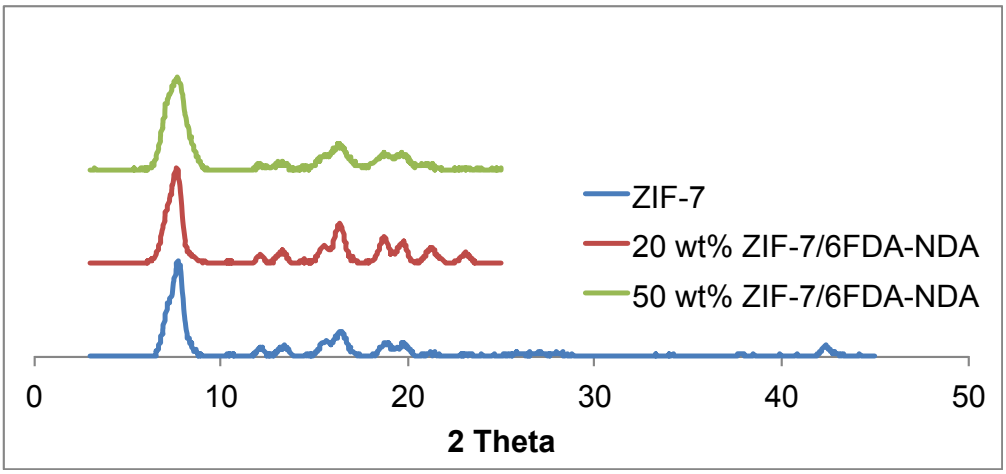

Figure 41. XRD patterns for ZIF-7/6FDA-NDA MMMs.

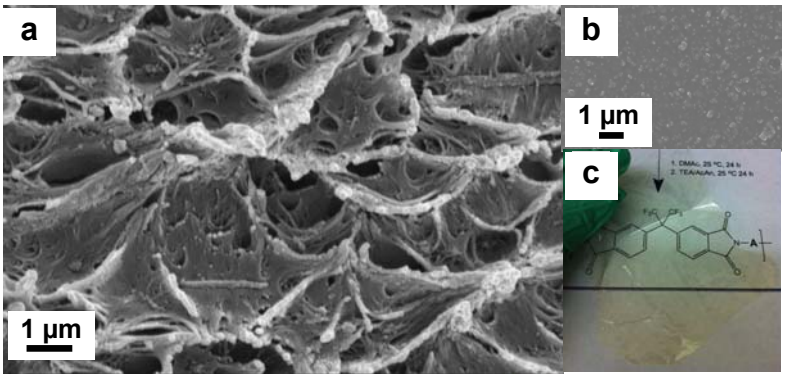

Figure 42. SEM images of the MMM (A) cross-section, (B) surface, and (C) optical image of a 25% (w/w) ZIF-7/6FDA-NDA-ODA (3:1) MMM.

Gas permeability testing of these MMMs showed increased permeabilities for all gases tested upon incorporation of ZIF-7 (Table 5). Increasing the ZIF-7 loading in 6FDA-NDA to 100% (w/w) increased both the hydrogen permeability and H_2/CO_2 selectivity (Table 6) placing this result on Robeson's upper bound (Figure 60). The 25% (w/w) ZIF-7/6FDA-NDA-ODA (3:1) MMM showed significantly improved performance for CO_2/CH_4 separations (Tables 5 and 6, Figure 60).

Table 5. Permeabilities (in Barrers) of ZIF-7/PI MMMs

	H_2	CO_2	CH_4	N_2	O_2
6FDA-NDA	48 ± 0.72	26 ± 0.25	0.58 ± 0.03	2.38 ± 0.15	6.67 ± 0.04
6FDA-NDA-ODA (1:3)	33 ± 2.0	16 ± 0.14	0.45 ± 0.01	0.68 ± 0.02	4.15 ± 0.09
25% (w/w) ZIF-7/6FDA-NDA-ODA	85 ± 4	47 ± 5	-	-	-
100% (w/w) ZIF-7/6FDA-NDA-ODA	200 ± 2	55 ± 2	-	-	-
25% (w/w) ZIF-7/6FDA-NDA-ODA (1:3)	93 ± 3	60 ± 1	0.92 ± 0.03	2.13 ± 0.01	6.2 ± 0.10

Table 6. Ideal selectivities of ZIF-7/PI MMMs

	H_2/CO_2	H_2/N_2	H_2/CH_4	H_2/O_2	CO_2/CH_4	CO_2/N_2
6FDA-NDA	1.8	20	84	7.2	46	11
6FDA-NDA-ODA (1:3)	2.06	49	73	8	36	24
25% (w/w) ZIF-7/6FDA-NDA-ODA	1.81	-	-	-	-	-
100% (w/w) ZIF-7/6FDA-NDA-ODA	3.6	-	-	-	-	-
25% (w/w) ZIF-7/6FDA-NDA-ODA (1:3)	1.55	44	101	15	65	28

ZIF-8/6FDA-durene and ZIF-8/6FDA-durene-EDA surface modification

XRD patterns of the ZIF-8 particles reacted with EDA vapor for 40 min (Figure 43) suggest that the crystal structure of ZIF-8 is intact after EDA exposure. The stability of the ZIF-8 functional groups to EDA vapor was verified by ATR-FTIR.

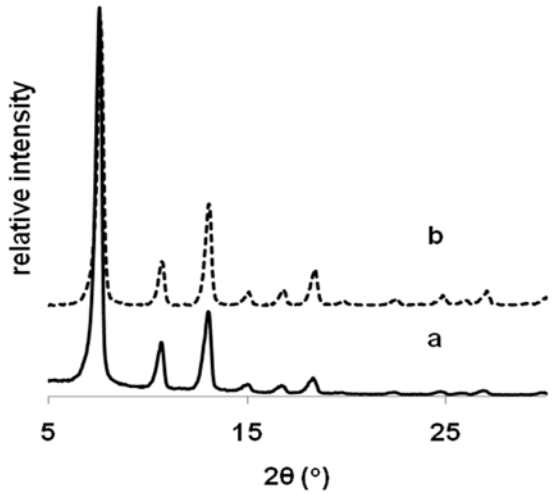

Figure 43. XRD patterns of (a) ZIF-8 and of (b) ZIF-8 exposed to EDA for 40 min and then dried at 70 °C for 12 h under vacuum.

An SEM image of the cross-section of a 50% (w/w) ZIF-8/6FDA-durene MMM reveals efficient wetting of the ZIF-8 particles by the polymer as evidenced by polymer veins (Figure 44a). An SEM image of the air-surface of the MMM demonstrates that the ZIF-8 nanoparticles have agglomerated into sub-micron sized particles in the 6FDA-durene polymer matrix (Figure 44b).

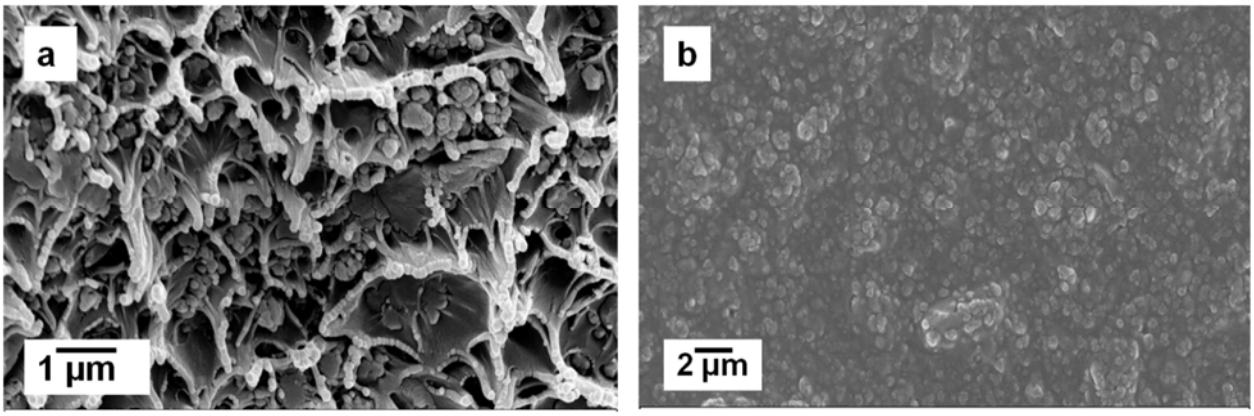

Figure 44. SEM images of (a) cross-section and (b) surface of a 50% (w/w) ZIF-8/6FDA-durene MMM.

After reacting the MMM with EDA vapor for 40 min, SEM revealed a dense skin with a thickness of ~10 ± 0.8 µm on both sides of the MMM (Figure 45), which can be attributed to cross-linking.

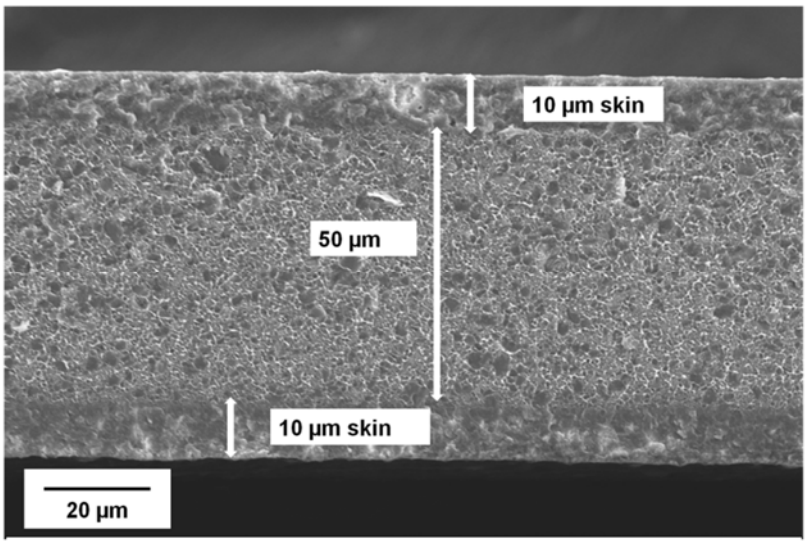

Figure 45. SEM image of a cross-section of a 50% (w/w) ZIF-8/6FDA-durene MMM after cross-linking with EDA for 40 min.

TGA plots of 6FDA-durene and the MMMs prior to reaction with EDA vapor showed thermal stability up to >400 ^{o}C (Figure 46). A weight loss of ~5% from 150-300 ^{o}C was observed for the EDA cross-linked MMM due to the elimination of diamine.

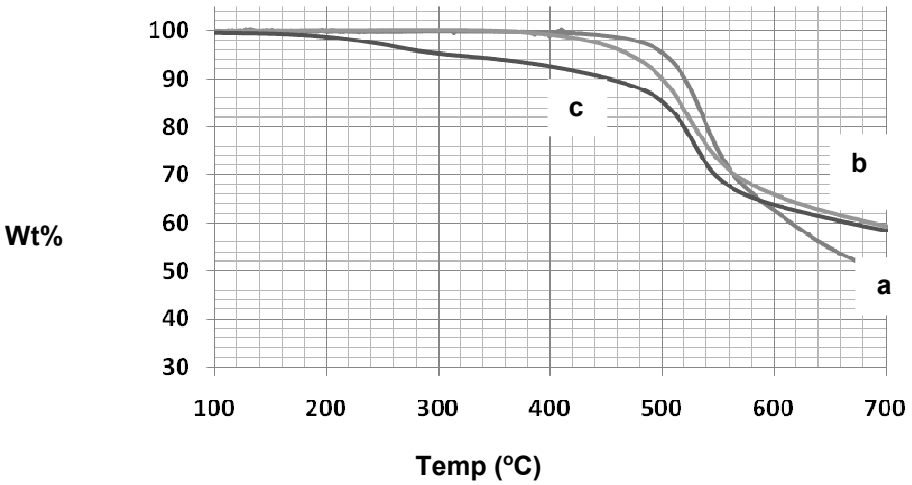

Figure 46. TGA of (a) 6FDA-durene, (b) 50% (w/w) ZIF-8/6FDA-durene MMM, and (c) 50% (w/w) ZIF-8/6FDA-durene MMM after reacting with EDA for 40 min.

The chemical modification that occurred to the MMM from exposure to EDA vapor was examined using ATR-FTIR spectroscopy. Distinctive bands were observed for the ZIF-8/6FDA-durene MMM (Figure 47a) at 1721 cm^{-1} (imide C=O symmetric stretch), 1781 cm^{-1} (imide C=O asymmetric stretch), and 1353 cm^{-1} (imide C-N stretch) due to the imide ring in 6FDA-durene. When exposed to EDA vapor for 40 min (Figure 47d), these bands disappeared, and peaks characteristic of the amide group appeared at 1671 cm^{-1} (amide C=O stretch) and 1524 cm^{-1} (amide C-N stretch). The band at 1253 cm^{-1} (C-F stretch) remained unchanged. Shifts in these IR bands are similar to those observed for EDA cross-linked 6FDA-durene, and demonstrate that the chemical reaction taking place during EDA vapor reaction is the ring-opening of the imide group in 6FDA-durene to an amide group followed by cross-linking.

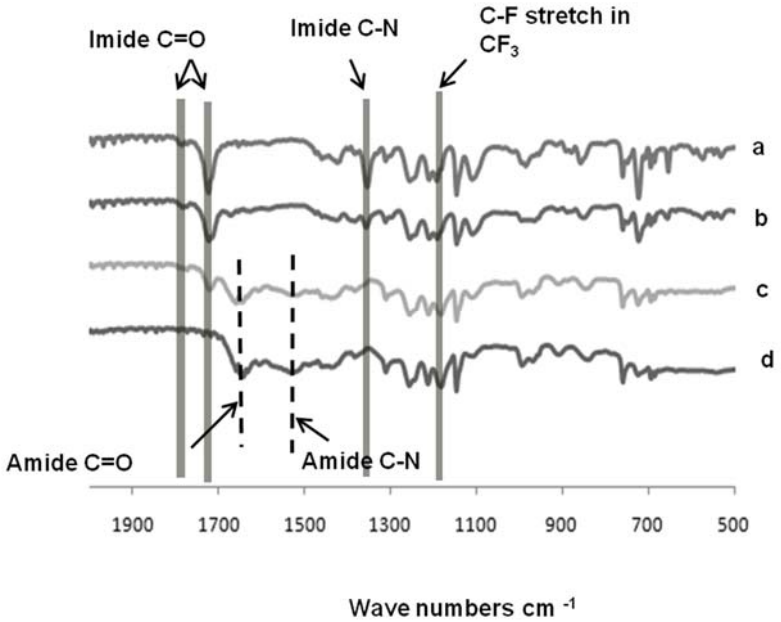

Figure 47. ATR-FTIR spectra of (a) 50% (w/w) ZIF-8/6FDA-durene MMM, (b) 50% (w/w) ZIF-8/6FDA-durene MMM treated with EDA for 40 min and annealed at 250 °C, (c) EDA treated MMM after annealing at 150 °C and (d) EDA treated MMM after annealing at 70 °C. (All membranes were annealed for 1 d).

A 50% (w/w) ZIF-8/6FDA-durene MMM showed small increases in H_2/CO_2 (from 1 to 1.4), H_2/N_2 (from 14.9 to 16), and O_2/N_2 (from 3.1 to 3.3) selectivities as compared to the unfilled polymer. An increase in gas permeability along with small enhancements in selectivity suggest good compatibility between ZIF-8 nanoparticles and 6FDA-durene with no major defects.

After cross-linking the MMM with EDA vapor, H_2 and O_2 permeabilities of the cross-linked MMM are 283.4 and 16.9 Barrers, respectively, which is 55% of the H_2 permeability and 16% of the O_2 permeability of 6FDA-durene. The observed CO_2, CH_4 and N_2 permeabilities were 5.5%, 4.7%, and 5.1% of those observed for 6FDA-durene (Table 7). Cross-linking led to one order of magnitude increases in selectivities for H_2/CO_2 (10.9 fold), H_2/N_2 (9.5 fold), and H_2/CH_4 (11.4 fold) separations, whereas O_2/N_2 selectivity increased by a factor of 2.7 in the cross-linked MMM as compared to 6FDA-durene (Table 8) [21].

Table 7. Permeability (Barrers) values for 6FDA-durene, 6FDA-durene cross-linked by reacting with EDA for 12 min, 50% (w/w) ZIF-8/6FDA-durene MMM, 50% (w/w) ZIF-8/6FDA-durene MMM cross-linked by reacting with EDA for 40 min, and the cross-linked skin of the MMM all measured at 35 °C and 3.5 atm [21]

Membrane	**Permeability (Barrers)**				
	H_2	**CO_2**	**N_2**	**CH_4**	**O_2**
6FDA-durene	518.5	468.5	34.9	30.0	107.7
Cross-linked 6FDA-durene	52.1	0.4	*	*	2.0
MMM	2136.6 ± 189.9	1552.9 ± 138.4	137.3 ± 17.6	140.3 ± 38.4	449.7 ± 100.2
Cross-linked MMM	283.5 ± 33.0	23.7 ± 2.8	2.0 ± 0.17	1.40 ± 0.13	16.9 ± 2.7
Cross-linked skin of MMM	89.4	6.8	0.58	0.40	5.0

* Permeability was too low to be detected

Table 8. Ideal gas selectivities for 6FDA-durene, 6FDA-durene cross-linked by reacting with EDA for 12 min, 50% (w/w) ZIF-8/6FDA-durene MMM, 50% (w/w) ZIF-8/6FDA-durene MMM cross-linked by reacting with EDA for 40 min, and the cross-linked skin of the MMM all measured at 35 °C and 3.5 atm [21]

Membrane	**Ideal gas selectivity**			
	H_2/CO_2	**H_2/N_2**	**O_2/N_2**	**H_2/CH_4**
6FDA-durene	1.1	14.9	3.1	17.9
Cross-linked 6FDA-durene	144	-	-	-
MMM	1.4 ± 0.0	16.0 ± 3.1	3.3 ± 0.14	15.3 ± 0.56
Cross-linked MMM	12.0 ± 0.07	141.4 ± 4.7	8.5 ± 2.1	203.3 ± 3.7
Cross-linked skin of MMM	13.1	155.0	8.6	222.1
Knudsen factor	4.7	3.7	0.9	2.8

After reacting the 50% (w/w) ZIF-8/6FDA-durene MMM with EDA vapor, SEM revealed a dense skin of ~10 ± 0.8 μm thickness on both sides of the MMM (Figure 48), which can be attributed to cross-linking.

When 6FDA-durene was spin coated onto annealed 50% (w/w) ZIF-8/6FDA-durene MMMs, a 2.7 ± 0.3 µm thick 6FDA-durene layer was observed by SEM (not shown). As shown in Figure 60, adding ZIF-8 to 6FDA-durene increased H_2 permeability to 2137 ± 190 Barrers, and EDA cross-linking of the MMM increased the H_2/CO_2 selectivity to 12 ± 0.07 while maintaining a moderate H_2 permeability. Asymmetric membranes having a thin cross-linked 6FDA-durene layer on a ZIF-8/6FDA-durene MMM showed a high H_2/CO_2 selectivity of 30.0 ± 3 with a high H_2 permeability close to the original permeability of 6FDA-durene.

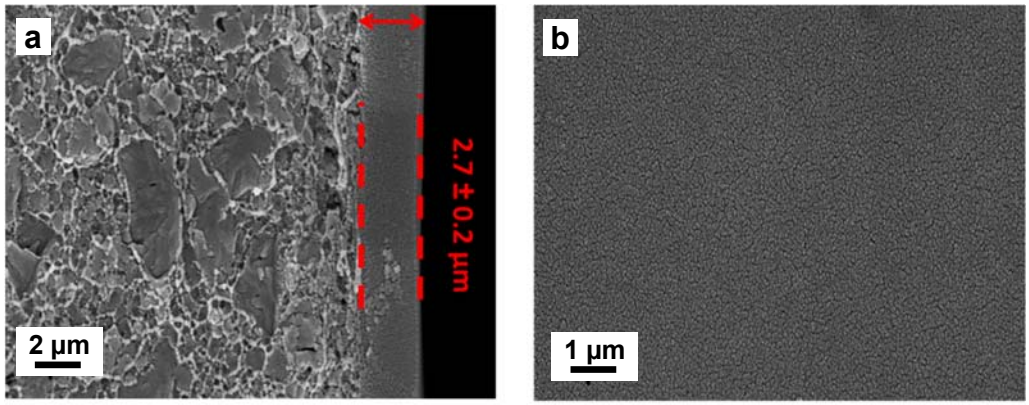

Figure 48. SEM image of a cross-section (a) and surface (b) of a 50% (w/w) ZIF-8/6FDA-durene MMM after cross-linking with EDA.

6FDA-DAM-DABA-based MMMs

The SEM image of a 50% (w/w) ZIF-8 /PDMC MMM (Figure 49a) shows good polymer-particle interaction as evident from the polymer vein morphology. Cross-linking the MMM changes this morphology to a flake-like structure where polymer veins are less evident (Figure 49b). The XRD patterns in Figure 50 verify the presence of ZIF-8 in the fabricated MMMs. Adding ZIF-8 to PDMC increased gas permeability for all the gases with no loss in CO_2/CH_4, H_2/CH_4, and H_2/N_2 gas selectivity (Table 9) placing the 50% (w/w) ZIF-8/CPDM MMM above the 2008 Robeson upper bound for the separation of H_2/CH_4 and H_2/N_2 and on or close to the upper bound for CO_2/CH_4 separations [22].

Cross-linking 50% (w/w) ZIF-8/PDMC to obtain 50% (w/w) ZIF-8/CPDM further enhanced the permeabilities of the gases, but was accompanied by decreases in CO_2/CH_4, H_2/CH_4, and H_2/N_2 gas selectivity (Table 9). The performance of the cross-linked MMM is above the 2008 Robeson upper bound for the separation of H_2/CH_4 and H_2/N_2 and on or close to the upper bound for CO_2/CH_4 separation [22]. As shown by TGA, the uncross-linked MMMs are stable up to 450 °C. The 10% weight loss starting from 200 °C is due to the removal of propanediol. The cross-linked MMMs are also stable up to 450 °C as shown in Figure 51.

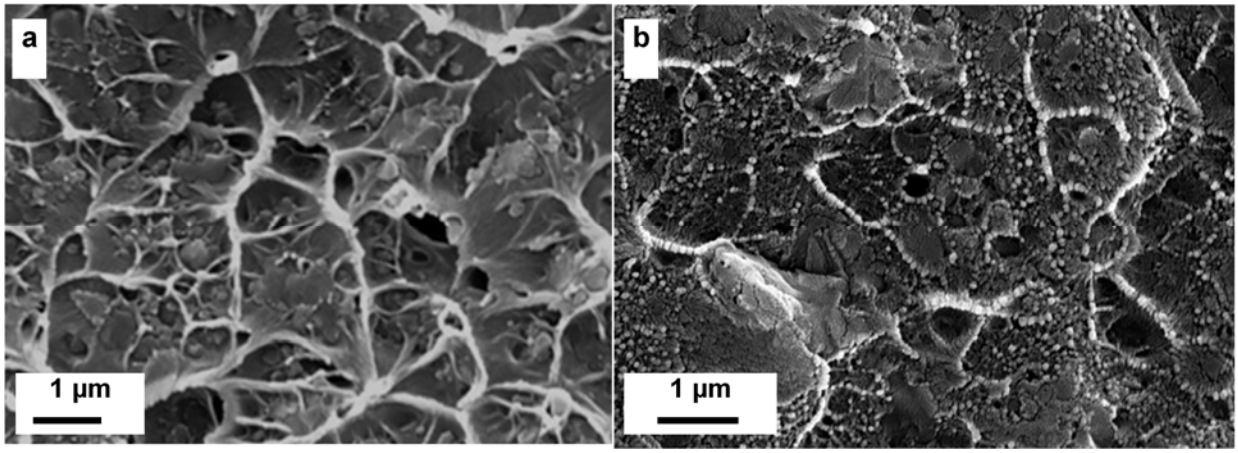

Figure 49. SEM images of cross-sections of (a) 50% (w/w) ZIF-8 /PDMC and (b) 50% (w/w) ZIF-8 /CPDM.

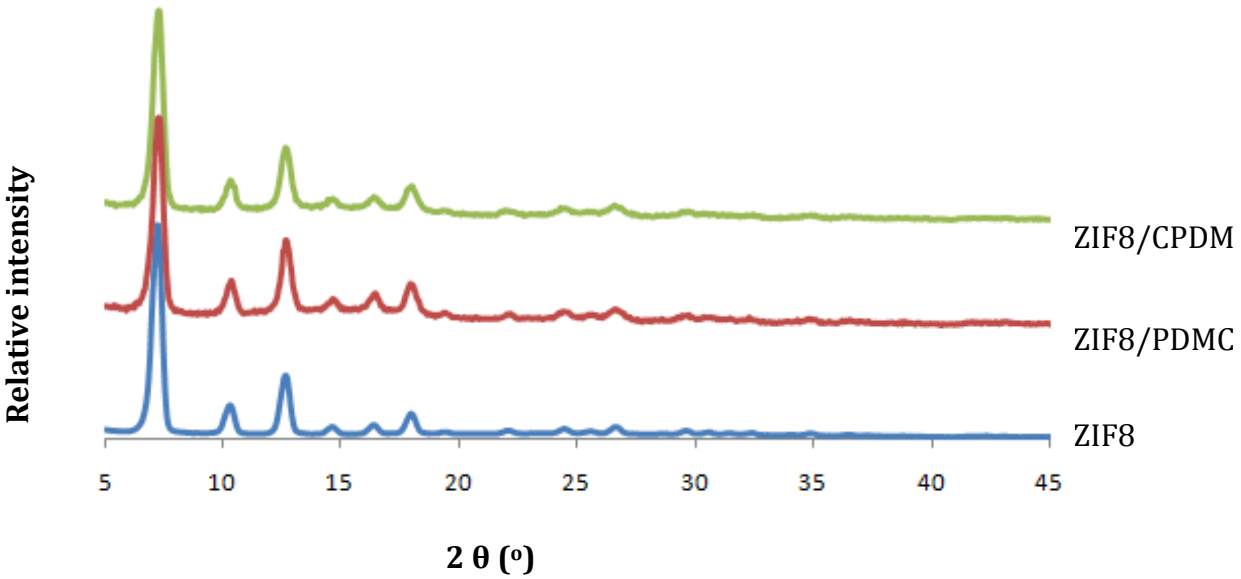

Figure. 50. XRD patterns for ZIF-8 and MMMs containing 50% (w/w) ZIF-8 loadings.

Table 9. Permeability data (Barrers) and selectivity for PDMC, CPDM and MMMs containing 50% (w/w) ZIF-8 loadings.

Membrane	Gas permeability (Barrer)				Gas pair selectivity		
	N_2	CH_4	CO_2	H_2	CO_2/CH_4	H_2/CH_4	H_2/N_2
PDMC	0.5	0.7	10.4	20.6	15.1	30.1	41.2
PDMC[23]	-	-	17.1	-	34.0	-	-
CPDM	-	2.4	91.7	159.0	37.9	65.7	-
CPDM[23]	-		77.3	-	39.9	-	-
Z8/PDMC	17.7	13.8	415.5	805.8	30.1	58.5	45.5
Z8/CPDM (210 °C)	29.6	24.7	484.9	995.5	19.6	40.2	33.6
Z8/CPDM (280 °C)	82.8	65.0	1230.3	1903.5	18.9	29.3	23.0

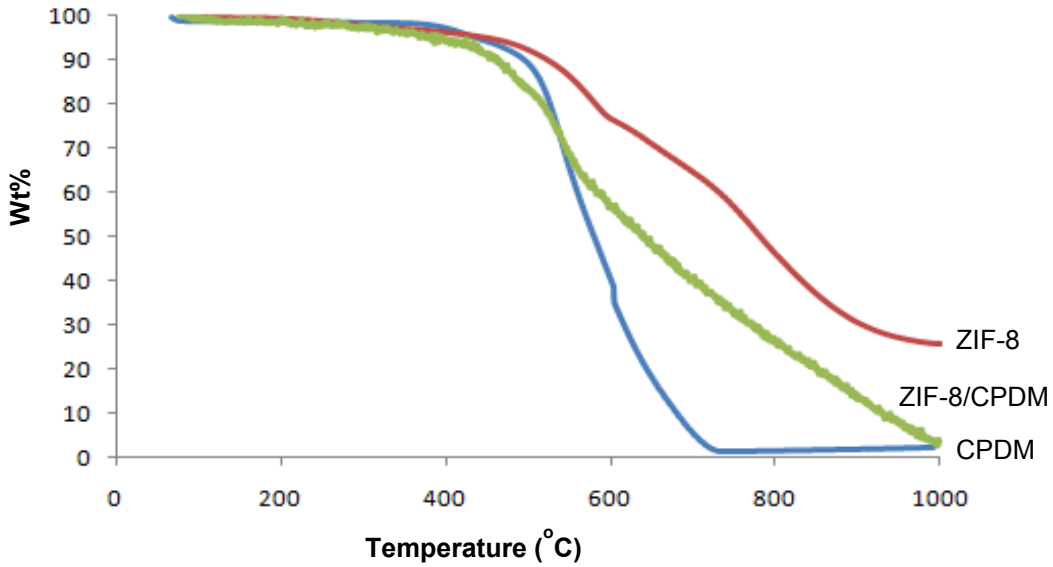

Figure 51. TGA plots of ZIF-8, CPDM and 50% (w/w) ZIF-8/CPDM MMMs.

VTEC PI-1388 membranes [17]

Figure 52 shows an optical image of a VTEC PI-1388 membrane. Table 10 shows the permeability, flux, and selectivity results for N_2, H_2, and CO_2 measured at pressures up to 30 atm and at temperatures of 35 °C and 300 °C. At these pressures and temperatures, the H_2/CO_2 selectivity remains constant. The effect of temperature on permeability is notable at high temperatures as seen in the Robeson plot (Figure 60). Although pressure does not affect permeability, it does influence the gas flux across the membrane [17].

When the effects of both pressure and temperature are combined, the H_2 flux increases 300 times from 0.02 $\mathrm{ft}^3_{\mathrm{STP}}\mathrm{h}^{-1}\mathrm{ft}^{-2}$ at 35 °C and 3 atm to 6.10 $\mathrm{ft}^3_{\mathrm{STP}}\mathrm{h}^{-1}\mathrm{ft}^{-2}$ at 300 °C and 30 atm. Experiments revealed that temperature had a greater contribution; a 10-fold increase in temperature induced a 32-fold increase in flux, whereas a 10-fold increase in pressure resulted in only a 9-fold increase in flux. These results suggest that VTEC PI-1388 is stable at high temperatures and high pressures and that the increase in permeability may arise from the relaxation of the packing of the polymer chains at high temperature. In addition, the significant increase in flux at high temperature and high pressure suggests that VTEC PI-1388 could be a good candidate for high pressure, high temperature H_2/CO_2 separations.

Figure 52. Optical image of VTEC PI-1388 membrane surface after thermal treatment.

Table 10. Permeability, flux, and selectivity in VTEC PI-1388 at different temperatures and pressures [17]

Temperature		35 °C				300 °C			
Pressure (atm)		3	10	20	30	3	10	20	30
Permeability[a] (Barrers)[b]	N_2	0.04 ± 0.002	0.04 ± 0.003	0.04 ± 0.004	0.04 ± 0.01	8.76 ± 0.01	8.11 ± 0.29	7.81 ± 0.12	7.98 ± 0.03
	H_2	3.89 ± 0.14	3.74 ± 0.13	3.68 ± 0.16	3.66 ± 0.13	139.00 ± 8.01	139.72 ± 9.22	129.93 ± 15.96	131.02 ± 9.11
	CO_2	0.74 ± 0.01	0.59 ± 0.01	0.52 ± 0.01	0.49 ± 0.01	26.49 ± 1.55	24.64 ± 0.24	23.99 ± 0.57	24.17 ± 0.37
Flux[a] ($ft^3_{(STP)}\ h^{-1}\ ft^{-2}$)	N_2	0.0002 ± 0.00004	0.0006 ± 0.0002	0.001 ± 0.0002	0.002 ± 0.00001	0.04 ± 0.01	0.12 ± 0.04	0.24± 0.06	0.37 ± 0.08
	H_2	0.02 ± 0.008	0.06 ± 0.01	0.11 ± 0.03	0.17 ± 0.04	0.64 ± 0.19	2.17 ± 0.65	4.06 ± 1.44	6.10 ± 1.84
	CO_2	0.003 ± 0.001	0.009 ± 0.002	0.02 ± 0.004	0.02 ± 0.005	0.12 ± 0.03	0.38 ± 0.10	0.74 ± 0.20	1.11 ± 0.25
Selectivity[a]	H_2/CO_2	5.29 ± 0.27	6.33 ± 0.34	7.16 ± 0.35	7.46 ± 0.52	5.25 ± 0.01	5.67 ± 0.32	5.41 ± 0.54	5.43 ± 0.46
	CO_2/N_2	16.35 ± 1.14	14.3 ± 0.64	13.24 ± 1.33	12.28 ± 1.94	3.03 ± 0.18	3.05 ± 0.08	3.08 ± 0.02	3.03 ± 0.004

[a] Permeability, flux, and selectivity calculated from the average of 2 membranes with thicknesses of 5 and 7 μm.

[b] $1\ \text{Barrer} = 10^{-10}\left(\frac{\text{cm}^3_{\text{STP}} \cdot \text{cm}}{\text{cm}^2 \cdot \text{s} \cdot \text{cmHg}}\right)$

MOP-18/Matrimid® MMMs

Temperature- and pressure-dependent permeation experiments (Table 11) revealed that for Matrimid® and MOP-18/Matrimid® membranes H_2 permeation increased by 100% when the temperature was increased from 35 to 70 °C. This trend can be attributed to a combination of increased kinetic energy for H_2 and the loosening of the polymer chain packing that reduces the energy required for H_2 to diffuse through the membrane. In the case of CO_2, the changes in permeability with changes in temperature are coupled to pressure changes. At 35 °C for both Matrimid® and the MOP-18/Matrimid® MMM, the CO_2 permeability increased 100% with a 10-fold increase in pressure resulting in membrane plasticization and loss of H_2/CO_2 selectivity. When the temperature was then increased to 70 °C, CO_2 permeability remained constant with pressure increments and the H_2/CO_2 selectivity was recovered, suggesting that plasticization of the membranes was reversed. The high pressure gas permeation experiments showed that MOP-18/Matrimid® MMMs were resilient and sufficiently mechanically robust to perform gas separations at high transmembrane pressures and that the incorporation of the MOP-18 molecules did not introduce defects in the membranes. From the temperature-pressure permeability experiments, it can be concluded that temperature has more of an effect than pressure on the gas separation properties of Matrimid® and MOP-18/Matrimid® MMMs. The H_2/CO_2 separation result of this MMM is shown in the Robeson plot (Figure 60).

Table 11. Permeability* (Barrers) of H_2 and CO_2 and H_2/CO_2 selectivity in Matrimid® and 30% (w/w) MOP-18/Matrimid® MMMs at 35 and 70 °C and at 3 and 30 atm.

	Matrimid®				30% (w/w) MOP-18/Matrimid®			
Temperature	**35 °C**		**70 °C**		**35 °C**		**70 °C**	
Pressure (atm)	**3**	**30**	**3**	**30**	**3**	**30**	**3**	**30**
H_2	22.1 ± 5.9	22.2 ± 1.4	40.4 ± 5.3	37.5 ± 3.6	22.7 ± 4.9	21.2 ± 3.5	55.5 ± 1.1	51.1 ± 3.2
CO_2	9.7 ± 2.6	18.7 ± 4.5	12.8 ± 3.2	15.48 ± 0.8	14.1 ± 3.2	25.0 ± 1.9	24.0 ± 0.8	25.1 ± 1.4
H_2/CO_2	2.27 ± 0.01	1.22 ± 0.25	3.22 ± 0.40	2.42 ± 0.11	1.61 ± 0.01	0.84 ± 0.07	2.3 ± 0.03	2.04 ± 0.01

*average of 2 membranes

ZIF-8/PBI MMMs

PBI-based MMMs containing different loadings of ZIF-8 (Sigma Aldrich, Basolite® Z1200) nanoparticles were fabricated as flexible membranes and characterized (Figure 53). XRD patterns of the MMMs show that the crystallinity of ZIF-8 is intact in the PBI polymer matrix (Figure 54). Figure 55 shows that these membranes are flexible even at high ZIF-8 loadings.

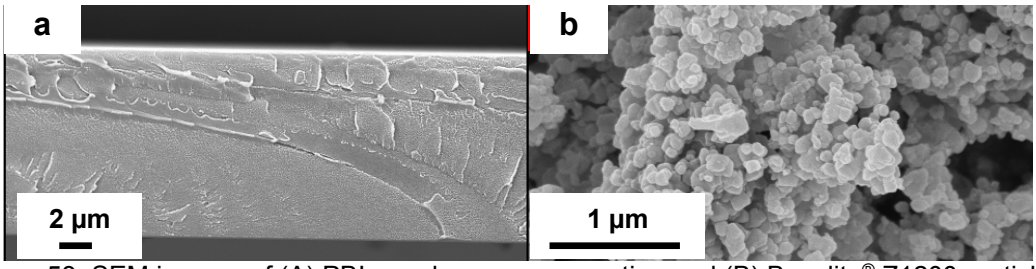

Figure 53. SEM images of (A) PBI membrane cross-section and (B) Basolite® Z1200 particles.

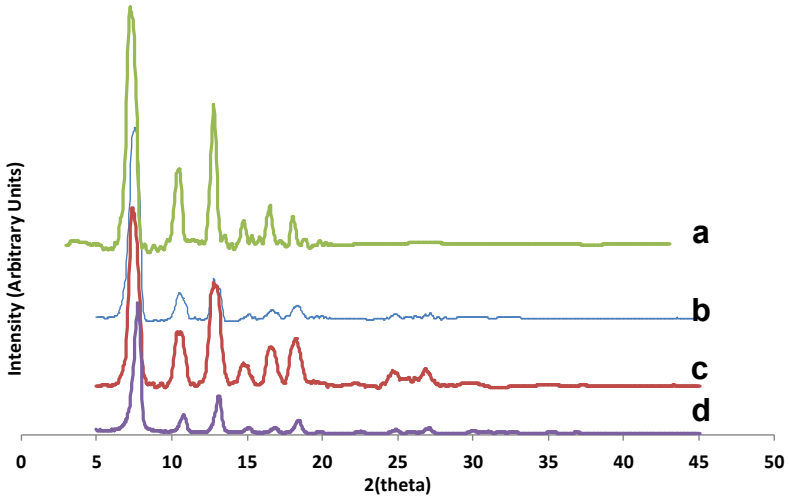

Figure 54. XRD patterns of ZIF-8/PBI MMMs at different ZIF loadings: (a) 75% (w/w), (b) 55% (w/w), and (c) 35% (w/w), (d) XRD pattern of ZIF-8 nanoparticles.

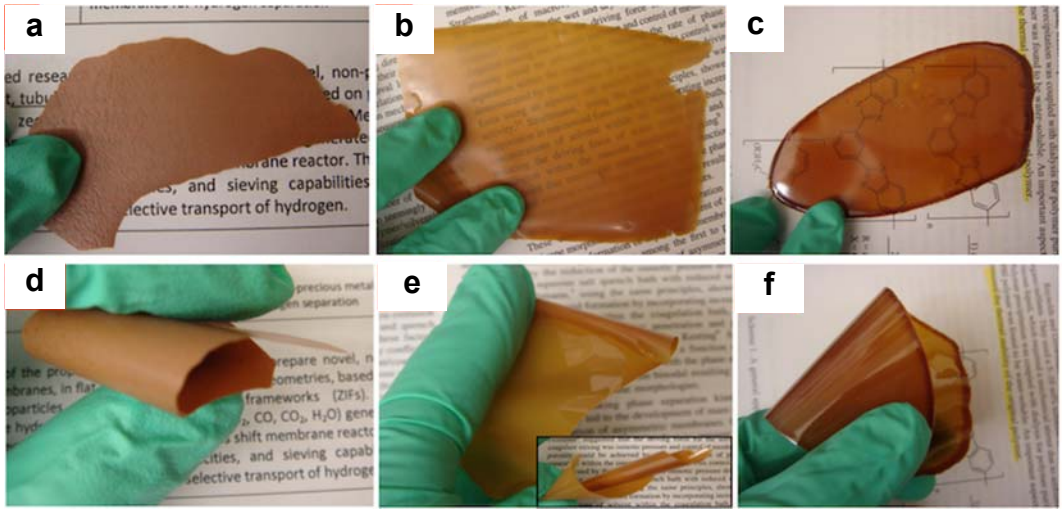

Figure 55. Optical images of ZIF-8/PBI MMMs at different ZIF loadings: (a), (d) 75% (w/w), (b), (e) 55% (w/w), and (c), (f) 35% (w/w) before annealing at 250 °C.

SEM images of cross-sections and surfaces of MMMs with several ZIF-8 loadings show that the ZIF-8 is uniformly dispersed after several cycles of stirring and sonication, followed by mixing in an acoustic mixer (Figure 56). Due to the nodular morphology of PBI, it is difficult to identify ZIF-8 in the PBI matrix. The annealing temperature of the MMMs significantly affected the gas permeability results. The 35% (w/w) ZIF-8/PBI MMM annealed at 250 °C showed a lower H_2 permeability than the MMM annealed at 180 °C, but displayed a H_2/CO_2 selectivity of 16. The permeabilities of the annealed MMMs are presented in Table 14. The XRD pattern did not change following annealing at 250 °C, and there were no peaks in the IR spectra that would indicate oxidation (not shown).

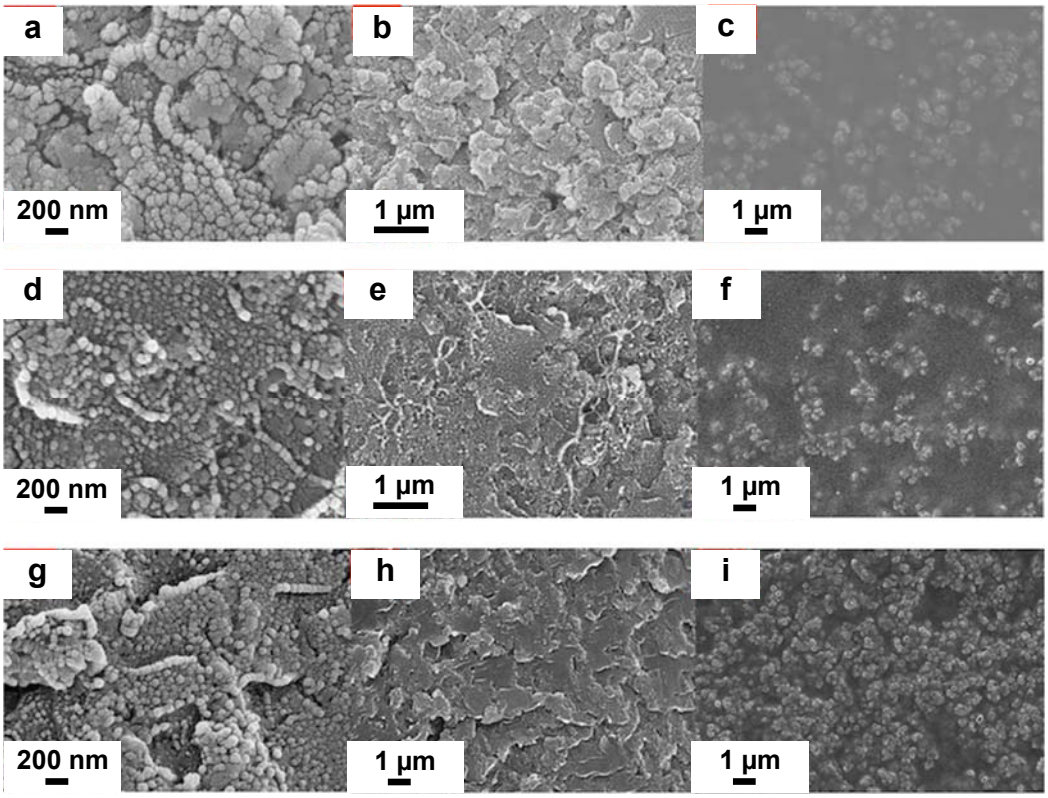

Figure 56. SEM images of MMM cross-sections (a, b, d, e, g, h) and surfaces (c, f, i) for different loadings of ZIF-8, a: 35% (w/w), b: 55% (w/w), c: 75% (w/w) in PBI after annealing at 250 °C.

A pure PBI membrane displayed a H_2/CO_2 selectivity of 24 and a H_2 permeability of 2.6 Barrers (Table 12). Increasing the ZIF-8 loading to 75% (w/w) in PBI increases the H_2 permeability, but decreases selectivity. Further increasing the loading to 122% (w/w) ZIF-8 decreased both the permeability and selectivity (data now shown), which could be attributed to the increased tortuosity of gas transport and/or blocked pores of ZIF-8. The permeability results lie close to Robeson's upper bound for H_2/CO_2 separations (Figure 60). Density measurements of these MMMs were performed to investigate the free volume changes that occur with increased ZIF loading (Table 13).

Table 12. Permeability and selectivity of ZIF-8/PBI MMMs with different loadings at 35 °C and 3 atm.

ZIF loading (w/w)	H_2	CO_2	H_2/CO_2
0	2.6 ± 0.12	0.11 ± 0.06	24
35	5.4 ± 0.70	0.33 ± 0.05	16
55	11.8 ± 0.12	1.6 ± 0.02	7
75	6.6 ± 0.10	1.3 ± 0.06	5

Table 13. Density measurements of MMMs by pycnometry using isooctanol as solvent.

ZIF loading (w/w)	Density, g/mL
0	1.30 ± 0.11
35	1.28 ± 0.03
55	1.26 ± 0.00
75	1.26 ± 0.01
ZIF-8	1.00 ± 0.02

The permeabilities of these MMMs were also measured at high temperatures (100 and 300 °C) and high pressures (up to 15 atm). An increase in permeability for the 35% (w/w) ZIF-8 loading was observed at 300 °C and 15 atm (Table 14), making this result above Robeson's upper bound line for the H_2/CO_2 separation (Figure 60).

Table 14. Permeability (Barrers) and selectivity of a 35% (w/w) ZIF-8/PBI MMM.

Temperature, °C	**35**	**300**	
Pressure, atm	**3**	**10**	**15**
H_2	5.4 ± 0.12	397 ± 9	397 ± 2
CO_2	0.33 ± 0.70	36 ± 0.15	29 ± 1
H_2/CO_2	16	11	14

Spin-coating of PBI layer

Figures 57 and 58 show SEM images of cross-sections of 35% (w/w) ZIF-8/PBI MMMs spin-coated with PBI layers of different thicknesses. The spin-coated PBI layer was thin, uniform, and dense, and its surface was typically defect free (Figure 57). A high magnification image (Figure 58) showed different morphologies for the PBI layer (left) and the 35% (w/w) ZIF-8/PBI MMM layer (right). The two layers appeared to interact well, and no voids were observed between the two layers. The thicknesses of the PBI layers were 950 nm (Figure 57) and 2.5 μm (Figure 58).

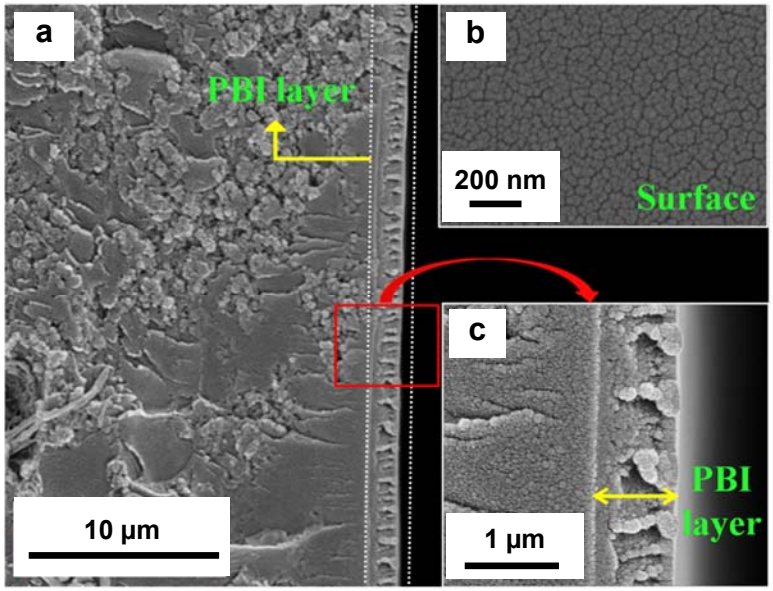

Figure 57. SEM images of a cross-section of a 35% (w/w) ZIF-8/PBI MMM with a 950 nm PBI skin (a). Inset shows image of surface (b) and a high magnification view (bottom) of the PBI layer (c).

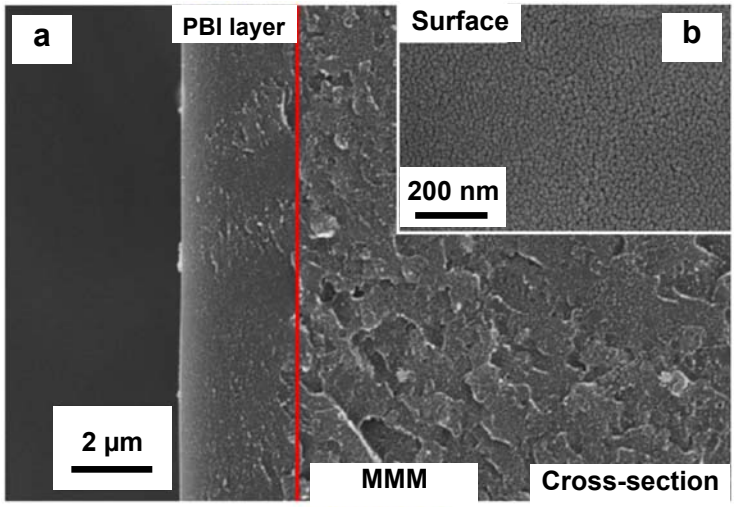

Figure 58. SEM image of a cross-section of a 35% (w/w) ZIF-8/PBI MMM spin-coated with a 2.5 µm PBI layer. Insert shows image of surface of PBI layer.

The 35% (w/w) ZIF-8/PBI MMM has lower H_2/CO_2 selectivity and higher H_2 and CO_2 permeability compared to the pure PBI membrane (Table 15). The gas separation properties of ZIF-8/PBI MMMs can be improved by coating with a very thin, dense, and uniform layer of PBI. In this structure, the thin PBI coating is the selective layer and the ZIF-8/PBI MMM contributes to the permeability. A 2.5 µm PBI layer increased H_2/CO_2 selectivity from 16 to 26.

Table 15. Gas permeation properties of 35% (w/w) ZIF-8/PBI MMM spin-coated with a 950 nm PBI layer. Permeability in Barrers.

	H_2	CO_2	H_2/CO_2
UTD-PBI (35 °C)	2.59	0.11	23
35% (w/w) ZIF-8/PBI MMM (35 °C)	5.36	0.33	16
35% (w/w) ZIF-8/PBI MMM with 950 nm PBI skin (35 °C)	4.13	0.31	13
35% (w/w) ZIF-8/PBI MMM with 2.5 µm PBI skin (35 °C)	4.16	0.16	26

For these MMMs with a PBI layer, the flux controls the properties of gas permeability and selectivity, as shown in Table 16. When the PBI skin was 950 nm, the flux of the PBI skin was higher than that of the MMM layer. As a result, the MMM with the 950 nm PBI layer exhibited gas permeability and selectivity similar to the uncoated MMM. However, when the PBI skin thickness was increased to 2.5 µm, the flux of the PBI skin was lower than the flux of the MMM layer, which led to a gas selectivity close to that of the pure PBI membrane.

Table 16. Flux (J) of 35% (w/w) ZIF-8/PBI MMM with PBI layer.

		950 nm PBI layer	**2.5 µm PBI layer**
PBI layer	**H_2**	50.0	17.9
	CO_2	2.34	0.836
MMM layer	**H_2**	35.1	29.2
	CO_2	2.16	1.80

Unit of flux = x 10^{-5} $\left(\frac{\mathrm{cm}^3_{\mathrm{STP}}}{\mathrm{cm}^2 \cdot \mathrm{s}}\right)$

ZIF-95/PBI and ZIF-95/6FDA-ODA-NDA MMMs

ZIF-95 is a chlorine-containing ZIF, which makes it incompatible with some high-performance polymers. The compatibility of ZIF-95 with PBI and 6FDA-ODA-NDA was tested. An optical image (not shown) of a 25% (w/w) ZIF-95/PBI MMM revealed separation between the ZIF-95 particles and the polymer matrix indicating poor compatibility and an optical image (not shown) of a 25% (w/w) ZIF-95/6FDA-ODA-NDA MMM showed a non-homogenous dispersion of ZIF-95. An SEM image of the 25% (w/w) ZIF-95/6FDA-ODA-NDA MMM (Figure 59) showed that the polymer did not wet the ZIF-95 additive.

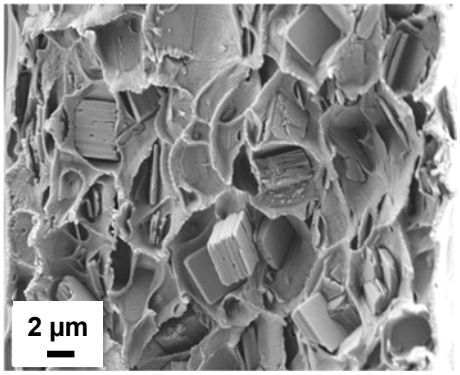

Figure 59. SEM image of 25% (w/w) ZIF-95/6FDA-ODA-NDA MMM.

High temperature and high pressure stability studies

The stability of several pure polymer and mixed-matrix membranes was tested by continuously exposing them to H_2, CO_2, N_2, and CH_4 at temperatures up to 300 °C and pressures up to 30 atm. Over 4,000 hours of testing was conducted with the longest individual test performed for over 300 hours.

Robeson plot of H_2/CO_2 separations

Table 17 provides a list of the membranes prepared in this project and Figure 60 presents the gas H_2/CO_2 separation results in the form of a Robeson plot. The plot combines of the results for membranes tested at 35, 70, and 300 °C.

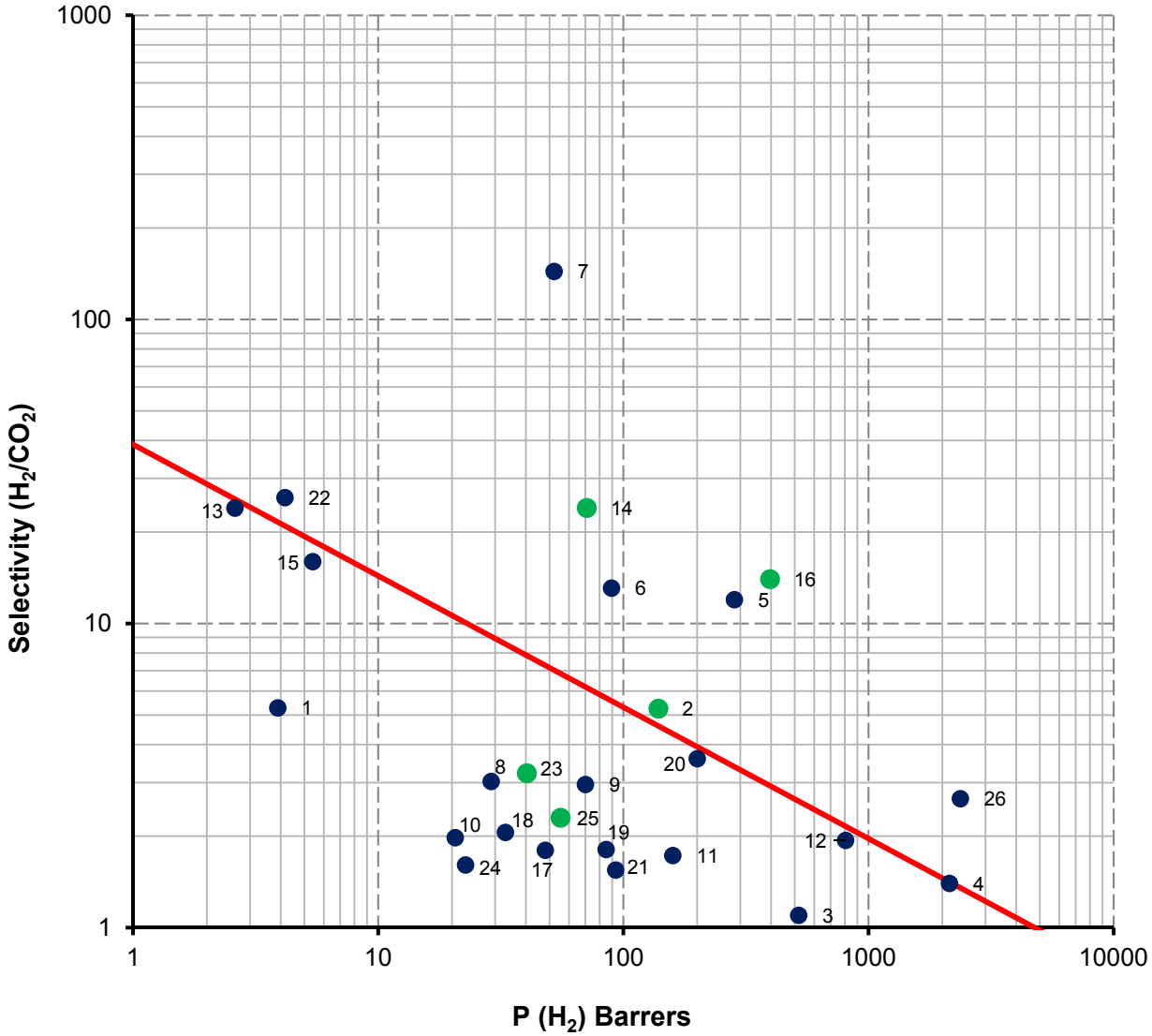

Figure 60. Robeson plot for H_2/CO_2 separations at 35, 70, and 300 °C [22]. Data points listed in Table 17.

Table 17. Gas transport properties of membranes

Membrane	#	PH_2	H_2/CO_2
VTEC PI-1388 [35 °C]	1	3.89	5.29
VTEC PI-1388 [300 °C]	2	139	5.25
6FDA-durene	3	518.5	1.1
50% (w/w) ZIF-8/6FDA-durene MMM	4	2136.6	1.4
50% (w/w) ZIF-8/6FDA-durene MMM EDA cross-linked	5	283.5	12
EDA cross-linked 6FDA-durene layer on 50% (w/w) ZIF-8/6FDA-durene MMM	6	89.4	13.1
EDA cross-linked 6FDA-durene	7	52.1	144
Matrimid® [35 °C]	8	28.88	3.03
40% (w/w) ZIF-8/Matrimid®	9	70	2.96
PDMC	10	20.6	1.98
CPDM	11	159	1.73
50% (w/w) ZIF-8/CPDM	12	805.8	1.94
PBI [35 °C]	13	2.6	24
PBI [300 °C]	14	71	24
35% (w/w) ZIF-8/PBI [35 °C]	15	5.4	16
35% (w/w) ZIF-8/PBI [300 °C]	16	397	14
6FDA-NDA	17	48	1.8
6FDA-NDA-ODA (1:3)	18	33	2.06
25% (w/w) ZIF-7/6FDA-NDA	19	85	1.81
100% (w/w) ZIF-7/6FDA-NDA	20	200	3.6
25% (w/w) ZIF-7/6FDA-NDA-ODA (1:3)	21	93	1.55
35% (w/w) ZIF-8/PBI with PBI layer [35 °C]	22	4.16	26
Matrimid® [70 °C]	23	40.4	3.22
30% (w/w) MOP-18/Matrimid® [35 °C]	24	22.7	1.61
30% (w/w) MOP-18/Matrimid® [70 °C]	25	55.5	2.3
30% (w/w) ZIF-7/Matrimid®	26	2368	2.66

RELEVANCE AND OUTCOME/IMPACTS

Students from different educational levels and backgrounds contributed in the project. Six high school students from the Plano Independent School District Scholar, NanoExplorer (Alan G. MacDiarmid NanoTech Institute), and Welch Summer Scholar programs were involved in different aspects of membrane preparation and characterization. A total of ten undergraduate students from different disciplines also gained experience in ZIF, MOF, hybrid materials, or polymer synthesis during their research terms. Four chemistry graduate students (3 Ph.D. and 1 M.S.) worked actively on different aspects of the project and mentored undergraduate and high school students as well. One graduate student has completed her Ph.D. dissertation related to the preparation and characterization of ZIF-containing mixed-matrix membranes.

The PI (Musselman) and co-PIs (Balkus, Ferraris) have actively disseminated the results of the project. A graduate course on *Special Topics in Materials Chemistry* focusing on *Membranes for Gas Separation* was taught in spring 2012. A chapter book review describing the current state of ZIFs and MOFs in mixed-matrix membranes was published in *Advanced Materials for Membrane Preparation* in 2011 [1]. Manuscripts describing the preparation and performance of ZIF-8/Matrimid® MMMs [18], the gas separation properties of cross-linked MMMs [21], and the construction of a high pressure, high temperature permeameter [17] have been published or submitted for publication, and several more manuscripts are in preparation. In addition, four conference proceedings on MMMs have been published [REFS]. The undergraduate and graduate students who worked on the project gave talks at the American Chemical Society local and national meetings and at the annual North American Membrane Society meetings. The PI also gave a plenary talk on mixed-matrix membranes at the North American Membrane Society meeting in New Orleans, LA, 2012. Talks at the University of Arkansas (February 2009) and the Southwest Catalysis Society Meeting (March 2009) were also given. The PIs also attended international conferences where they gave talks at the Global Partnership Program at Hanyang University in Korea (March 2010), a plenary lecture at XVII Zeolite Forum in Poznan, Poland (May 2010), the 5th International Zeolite Membrane Meeting in Loutraki, Greece (May 2010), and the 16th International Zeolite Conference in Sorento-Naples, Italy (July 2010).

CONCLUSIONS

Nanoparticles of ZIFs, MOFs, and related hybrid materials were successfully prepared by modifying published procedures by introducing bases, changing stoichiometric ratios, or adjusting reaction conditions. These materials displayed high thermal stabilities (up to 500 ^{o}C) and the expected X-ray patterns. The synthesized ZIFs included ZIF-7, ZIF-8, ZIF-20, and ZIF-90, while the MOFs and other hybrid materials included MIL-53, NH_2-MIL-53, and MOP-18. These materials were incorporated into thermally stable commercial and synthesized polymers and investigated for their gas separation properties.

ZIF-8/Matrimid® MMMs were cross-linked with EDA vapor to enhance the selectivity properties of the membranes. ZIF-8/Matrimid® MMMs were also spin-coated with a Matrimid® layer, which was cross-linked with EDA vapor resulting in a surface layer or skin on the MMM. Gas permeabilities increased for the cross-linked ZIF-8/Matrimid® MMMs, which was attributed to defects formed during cross-linking resulting in gas selectivities close to Knudsen values. The permeabilities for the cross-linked, spin-coated Matrimid® ZIF-8/Matrimid® MMMs decreased for all gases tested and increases in selectivities for H_2/CO_2, H_2/N_2, H_2/O_2, and H_2/CH_4 gas pairs were observed compared to those of uncross-linked ZIF-8/Matrimid® MMMs, which was attributed to a reduction in the diffusive pathways for the larger gas molecules. The gas separation properties of the cross-linked, spin-coated Matrimid® ZIF-8/Matrimid® MMMs lie close to the Robeson's upper bound.

Thermally stable 6FDA-based polyimide polymers were prepared with high molecular weights (at least 60,000 Da): 6FDA-NDA, 6FDA-ODA and three of their copolymers (3:1, 1:1, 1:3 NDA-ODA). These polymers showed high thermal stabilities up to 450 ^{o}C. Incorporation of ZIF-7 into 6FDA-NDA resulted in increased hydrogen permeabilities at 25% (w/w) and 100% (w/w) loadings. A 100% (w/w) ZIF-7/6FDA-NDA MMM displayed increases in both H_2 permeability and H_2/CO_2 selectivity at 35 ^{o}C and 3 atm. Adding a 50% (w/w) loading of nanocrystalline ZIF-8 to 6FDA-durene resulted in an approximately 400% increase in hydrogen permeability with a modest increase in H_2/CO_2 selectivity as compared to 6FDA-durene. EDA cross-linking rendered ~10-fold increases in H_2/CO_2 selectivity with respect to 6FDA-durene. The H_2/CO_2 selectivity for the cross-linked MMM was 12 and the hydrogen permeability was 283.4. Cross-linking the asymmetric 50% (w/w) ZIF-8/6FDA-durene further improved both the H_2/CO_2 selectivity and H_2 permeability as compared to the EDA treated MMM, yielding a high H_2/CO_2 selectivity of 30 and a H_2 permeability close to pure 6FDA-durene.

PIM-1 was synthesized with a high molecular weight of 126,000 Da and a PDI of 2.7. Commercially available ZIF-8 and MIL-53 particles were incorporated into PIM-1 with loadings up to 17.6% (w/w). These MMMs showed increased permeabilities for H_2, CO_2, and CH_4, without any improvements in selectivities.

A high pressure, high temperature (HPHT) permeameter was constructed for this project. Using the HPHT permeameter, the permeabilities of N_2, H_2, and CO_2 in VTEC PI-1388 were measured at pressures up to 30 atm and at temperatures up to 300 °C. For VTEC PI-1388, it was found that higher temperatures induce greater changes in gas flux than do higher pressures. The HPHT results and the long term stability studies (300 h at 300 °C) indicate that VTEC PI-1388 is a resilient polymer that may suitable for H_2/CO_2 separations at high pressure and high temperature. The polymer retained its H_2/CO_2 separation of 5.43 with a H_2 permeability of 131 Barrers at 30 atm and 300 °C.

High pressure and high temperature gas permeation experiments for MOP-18/Matrimid® MMMs revealed that CO_2 plasticizes the membranes at 35 °C and 30 atm reducing H_2/CO_2 selectivity. Plasticization was reversed when the temperature was increased to 70 °C and the H_2/CO_2 selectivity was recovered for feed pressures of 3 and 30 atm.

MMMs were fabricated using PBI and different loadings of commercially available ZIF-8 (Basolite® Z1200). Compared to pure PBI, hydrogen permeability increased up to 12 Barrers at 55% (w/w) and H_2/CO_2 selectivity was highest at the 35% (w/w) loading. Testing of the 35% (w/w) MMM at 300 ^{o}C and 15 atm showed a 70-fold increase in hydrogen permeability with a minimal loss in H_2/CO_2 selectivity. These results lie beyond Robeson's upper bound line for H_2/CO_2 separations.

REFERENCES

[1] Ferraris, J. P.; Musselman, I. H.; Kenneth J. Balkus, J., Mixed matrix membranes based on metal organic frameworks. In *Advanced Materials for Membrane Preparation*, Buonomenna, M. G., Ed. Bentham Science: Rende, Italy, 2012; Vol. 1, pp 83-93.

[2] Huang, X.; Zhang, J.; Chen, X., $[Zn(bim)_2]\cdot(H_2O)_{1.67}$: A metal-organic open-framework with sodalite topology. *Chin. Sci. Bull.* **2003,** 48, (15), 1531-1534.

[3] Hayashi, H.; Cote, A. P.; Furukawa, H.; O'Keeffe, M.; Yaghi, O. M., Zeolite A imidazolate frameworks. *Nat. Mater.* **2007,** 6, (7), 501-506.

[4] Song, Q.; Nataraj, S. K.; Roussenova, M. V.; Tan, J. C.; Hughes, D. J.; Li, W.; Bourgoin, P.; Alam, M. A.; Cheetham, A. K.; Al-Muhtaseb, S. A.; Sivaniah, E., Zeolitic imidazolate framework (ZIF-8) based polymer nanocomposite membranes for gas separation. *Energy & Environmental Science* **2012,** 5, (8), 8359-8369.

[5] Morris, W.; Doonan, C. J.; Furukawa, H.; Banerjee, R.; Yaghi, O. M., Crystals as molecules: postsynthesis covalent functionalization of zeolitic imidazolate frameworks. *J. Am. Chem. Soc.* **2008,** 130, 12626-12627.

[6] Wang, B.; Cote, A. P.; Furukawa, H.; O'Keeffe, M.; Yaghi, O. M., Colossal cages in zeolitic imidazolate frameworks as selective carbon dioxide reservoirs. *Nature* **2008,** 453, (7192), 207-211.

[7] Loiseau, T.; Serre, C.; Huguenard, C.; Fink, G.; Taulelle, F.; Henry, M.; Bataille, T.; Ferey, G., A rationale for the large breathing of the porous aluminum terephthalate (MIL-53) upon hydration. *Chem. Eur. J.* **2004,** 10, (6), 1373-1382.

[8] Pera-Titus, M.; Savonnet, M.; Farrusseng, D., Evaluation of Energy Heterogeneity in Metal Organic Frameworks: Absence of Henry's Region in MIL-53 and MIL-68 Materials? *J. Phys. Chem. C* **2010,** 114, (41), 17665-17674.

[9] Furukawa, H.; Kim, J.; Plass, K. E.; Yaghi, O. M., Crystal structure, dissolution, and deposition of a 5 nm functionalized metal-organic great rhombicuboctahedron. *J. Am. Chem. Soc.* **2006,** 128, (26), 8398-8399.

[10] Ahn, J.; Chung, W. J.; Pinnau, I.; Song, J.; Du, N.; Robertson, G. P.; Guiver, M. D., Gas transport behavior of mixed-matrix membranes composed of silica nanoparticles in a polymer of intrinsic microporosity (PIM-1). *J. Membr. Sci.* **2010,** 346, (2), 280-287.

[11] Song, J.; Du, N.; Dai, Y.; Robertson, G. P.; Guiver, M. D.; Thomas, S.; Pinnau, I., Linear high molecular weight ladder polymers by optimized polycondensation of tetrahydroxytetramethylspirobisindane and 1,4-dicyanotetrafluorobenzene. *Macromolecules* **2008,** 41, (20), 7411-7417.

[12] Chan, S. S.; Chung, T. S.; Liu, Y.; Wang, R., Gas and hydrocarbon (C2 and C3) transport properties of co-polyimides synthesized from 6FDA and 1,5-NDA (naphthalene)/Durene diamines. *J. Membr. Sci.* **2003,** 218, (1-2), 235-245.

[13] Widjojo, N.; Chung, T. S., Pervaporation dehydration of C_2-C_4 alcohols by 6FDA-ODA-NDA/Ultem dual-layer hollow fiber membranes with enhanced separation performance and swelling resistance. *Chem. Eng. J.* **2009,** 155, (3), 736-743.

[14] Liu, Y.; Wang, R.; Chung, T. S., Chemical cross-linking modification of polyimide membranes for gas separation. *J. Membr. Sci.* **2001,** 189, 231-239.

[15] Hillock, A. M. W.; Miller, S. J.; Koros, W. J., Crosslinked mixed matrix membranes for the purification of natural gas: Effects of sieve surface modification. *J. Membr. Sci.* **2008,** 314, (1-2), 193-199.

[16] Omole, I. C.; Miller, S. J.; Koros, W. J., Increased Molecular Weight of a Cross-Linkable Polyimide for Spinning Plasticization Resistant Hollow Fiber Membranes. *Macromolecules* **2008,** 41, (17), 6367-6375.

[17] Perez, E. V.; Kenneth J. Balkus, J.; Ferraris, J. P.; Musselman, I. H., Instrument for gas permeation measurements at high pressure and high temperature. *Rev. Sci. Instrum.* **2013,** Submitted.

[18] Ordoñez, M. J. C.; Balkus Jr, K. J.; Ferraris, J. P.; Musselman, I. H., Molecular sieving realized with ZIF-8/Matrimid® mixed-matrix membranes. *J. Membr. Sci.* **2010,** 361, (1-2), 28-37.

[19] Huang, A.; Chen, Y.; Wang, N.; Hu, Z.; Jiang, J.; Caro, J., A highly permeable and selective zeolitic imidazolate framework ZIF-95 membrane for H_2/CO_2 separation. *Chem. Commun.* **2012,** 48, 10981-10983.

[20] Schimtz, B.; Muller, U.; Trukhan, N.; Schubert, M.; Ferey, G.; Hirscher, M., Heat of adsorption for hydrogen in microporous high-surface area materials. *Chemical Physics & Physical Chemistry* **2008,** 9, 2181-2184.
[21] Wijenayake, S. N.; Panapitiya, N. P.; Versteeg, S. H.; Nguyen, C. N.; Goel, S.; Balkus, J. K. J.; Musselman, I. H.; Ferraris, J. P., Surface cross-linking of ZIF-8/polyimide mixed matrix membranes (MMMs) for gas separation. *Ind. Eng. Chem. Res.* **2013**.
[22] Robeson, L. M., The upper bound revisited. *J. Membr. Sci.* **2008,** 320, (1-2), 390-400.
[23] Hillock, A. M. W.; Koros, W. J., Cross-Linkable Polyimide Membrane for Natural Gas Purification and Carbon Dioxide Plasticization Reduction. *Macromolecules* **2007,** 40, (3), 583-587.

LIST OF ACRONYMS AND ABBREVIATIONS

Abbreviation	Description
6FDA	4,4'-hexafluoroisopropylidene bisphthalic dianhydride
ATR	Attenuated total reflectance
CPDM	Cross-linked propanediol monoester
DABA	3,5-diamino benzoic acid
DAM	2,4,6,-trimethyl-1,3-phenylene diamine
DMAc	Dimethylacetamide
DMF	Dimethylformamide
DSC	Differential scanning calorimetry
EDA	Ethylenediamine
FTIR	Fourier transform infrared
GPC	Gel permeation chromatography
HPHT	High pressure, high temperature
kDa	kilo Dalton
LiCl	Lithium chloride
MIL-53	Materials Institute Lavoisier 53
MIL-53-ht	Materials Institute Lavoisier 53 high temperature
MIL-53-lt	Materials Institute Lavoisier 53 low temperature
μm	Micrometer
MMM	Mixed-matrix membrane
Mn	Molecular number
MOF	Metal-organic framework
MOP-18	Metal-organic polyhedra 18
Mw	Molecular weight
NDA	1,5-diaminonaphthalene
NH_2-MIL-53	Amine functionalized Materials Institute Lavoisier 53
Nm	Nanometer
ODA	4,4'-Oxydianiline
PBI	Polybenzimidazole
PDI	Polydispersity index
PDMC	Propanediol monoester cross-linkable
PIM	Polymer of intrinsic microporosity
SEM	Scanning electron microscope
T_d	Temperature of decomposition
TEA	Triethylamine
T_g	Glass transition temperature
TGA	Thermogravimetic analysis
THF	Tetrahydrofuran
XRD	X-ray diffraction
ZIF	Zeolitic imidazolate framework